HHS Public Access

Author manuscript

Cell Rep. Author manuscript; available in PMC 2019 December 02.

Published in final edited form as:

Cell Rep. 2019 November 19; 29(8): 2270–2283.e7. doi:10.1016/j.celrep.2019.10.042.

Intestinal IL-17R Signaling Constrains IL-18-Driven Liver Inflammation by the Regulation of Microbiome-Derived Products

Patricia Castillo-dela Cruz[1,2], **Alanna G. Wanek**[3], **Pawan Kumar**[1,7], **Xiaojing An**[4], **Waleed Elsegeiny**[1,8], **William Horne**[1], **Adam Fitch**[4,5], **Ansen H.P. Burr**[1,2], **Kathyayini P. Gopalakrishna**[1,6], **Kong Chen**[4], **Barbara A. Methé**[4,5], **Scott W. Canna**[1,2], **Timothy W. Hand**[1,2], **Jay K. Kolls**[1,3,9,*]

[1]Richard King Mellon Foundation Institute for Pediatric Research, Department of Pediatrics, UPMC Children's Hospital of Pittsburgh, Pittsburgh, PA 15224, USA

[2]Department of Immunology, University of Pittsburgh School of Medicine, Pittsburgh, PA 15213, USA

[3]Departments of Medicine and Pediatrics, Center for Translational Research in Infection and Inflammation, Tulane University School of Medicine, New Orleans, LA 70112, USA

[4]Department of Medicine, Division of Pulmonary, Allergy, and Critical Care Medicine, University of Pittsburgh School of Medicine, Pittsburgh, PA 15213, USA

[5]Center for Medicine and the Microbiome, University of Pittsburgh School of Medicine, Pittsburgh, PA 15213, USA

[6]Department of Human Genetics, University of Pittsburgh Graduate School of Public Health, Pittsburgh, PA 15213, USA

[7]Present address: Department of Molecular Genetics and Microbiology, Stony Brook University, Stony Brook, NY 11794, USA

[8]Present address: Laboratory of Clinical Immunology and Microbiology, NIAID, NIH, Bethesda, MD 20892, USA

[9]Lead Contact

SUMMARY

Interleukin (IL)-17 signaling to the intestinal epithelium regulates the intestinal microbiome. Given the reported links between intestinal dysbiosis, bacterial translocation, and liver disease, we

*Correspondence: jkolls1@tulane.edu.

AUTHOR CONTRIBUTIONS

Conceptualization, P.C.-d.C., T.W.H., and J.K.K.; Methodology, P.C.-d.C., T.W.H., and J.K.K.; Formal Analysis, P.C.-d.C., A.G.W., A.H.P.B., K.P.G., K.C., Z.A., W.H., A.F., and B.A.M.; Investigation, P.C.-d.C., P.K., W.E., and Z.A.; Data Curation, A.G.W., W.H., A.F., and B.A.M.; Visualization, P.C.-d.C., A.G.W., T.W.H., and J.K.K.; Resources, S.W.C., T.W.H., and J.K.K.; Writing, P.C.-d.C., T.W.H., and J.K.K.; Supervision and Funding Acquisition, T.W.H. and J.K.K.

DECLARATION OF INTERESTS

The authors declare no competing interests.

SUPPLEMENTAL INFORMATION

Supplemental Information can be found online at https://doi.org/10.1016/j.celrep.2019.10.042.

hypothesize that intestinal IL-17R signaling plays a critical role in mitigating hepatic inflammation. To test this, we study intestinal epithelium-specific IL-17RA-deficient mice in an immune-driven hepatitis model. At the naive state, these mice exhibit microbiome dysbiosis and increased translocation of bacterial products (CpG DNA), which drives liver IL-18 production. Upon disease induction, absence of enteric IL-17RA signaling exacerbates hepatitis and hepatocyte cell death. IL-18 is necessary for disease exacerbation and is associated with increased activated hepatic lymphocytes based on *Ifng* and *Fasl* expression. Thus, intestinal IL-17R regulates translocation of TLR9 ligands and constrains susceptibility to hepatitis. These data connect enteric Th17 signaling and the microbiome in hepatitis, with broader implications on the effects of impaired intestinal immunity and subsequent release of microbial products observed in other extra-intestinal pathologies.

In Brief

Castillo-dela Cruz et al. describe a unique protective role of intestinal IL-17RA in hepatitis. Disruption of intestinal IL-17RA signaling results in microbiome dysbiosis and translocation of bacterial products, specifically unmethylated CpG DNA, to the liver. This promotes IL-18 production and subsequent lymphocyte activation and cell death to exacerbate liver inflammation.

Graphic Abstract

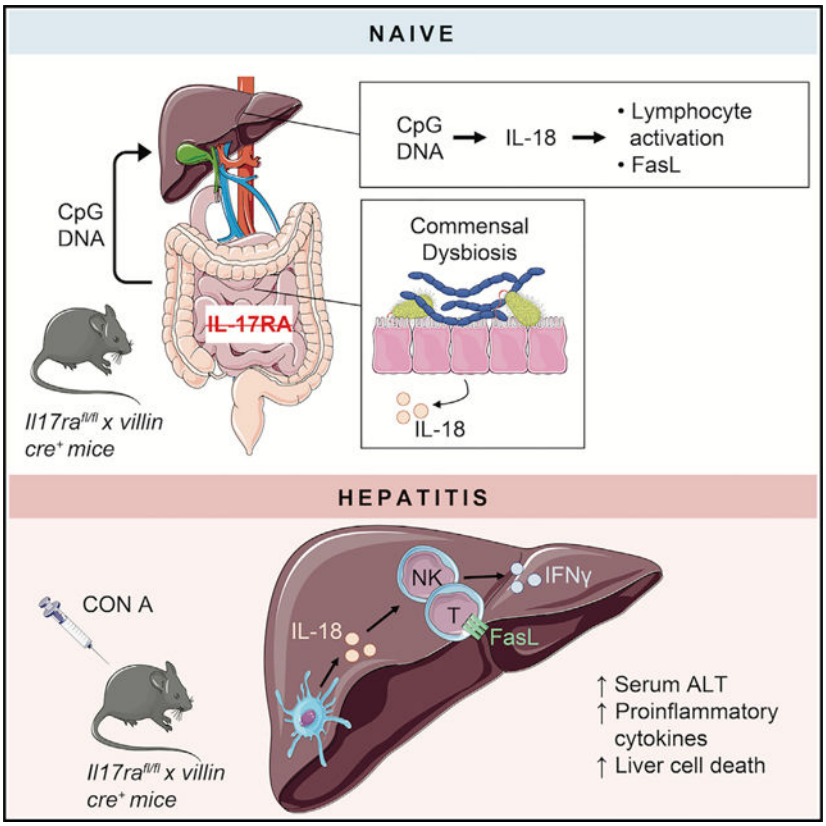

INTRODUCTION

T helper 17 (Th17) cells play a critical role in regulating the intestinal microbiome. Within the intestine, interleukin (IL)-17 primarily signals through epithelial cells. Correspondingly, epithelial-adherent bacteria, such as segmented filamentous bacteria (SFB), both induce and are controlled by IL-17 produced by T cells (Atarashi et al., 2015; Ivanov et al., 2009; Kumar et al., 2016). Th17 cells regulate the microbiome through a variety of mechanisms including induction of anti-microbial peptides (AMPs), reactive oxygen species, and immunoglobulin A (IgA) (Belkaid and Hand, 2014; Cao et al., 2012; Kolls et al., 2008; Kumar et al., 2016). These functions act together with other Th17 cytokines to maintain intestinal barrier integrity and homeostasis (Lee et al., 2015; Schreiber et al., 2015; Shih et al., 2014; Wang et al., 2017).

There is now a growing body of research linking alterations in the intestinal microbiome to liver pathologies. For example, patients with viral and autoimmune hepatitis exhibit intestinal dysbiosis (Aly et al., 2016; Lin et al., 2015). In mouse models of these diseases, manipulation of the microbiome through antibiotics ameliorated liver inflammation (Chen et al., 2014). Given the closely related vasculature of the liver and intestine, there is a normal physiological flux of bacterial products to the liver through the portal vein draining the intestine (Macpherson et al., 2016). Indeed, many models of liver inflammation have been associated with increased bacterial translocation (Chen et al., 2014; Henao-Mejia et al., 2013; Li et al., 2017; Lin et al., 2015; Pan et al., 2012; Yan and Schnabl, 2012). While there are data showing that bacterial traffic through the hepatic circulation activates toll-like receptors (TLRs) (Chassaing et al., 2014; Henao-Mejia et al., 2013), it is not fully understood how translocation of intestinal-resident bacteria/bacterial products affect local hepatic immune cell populations. Given the importance of IL-17R in intestinal homeostasis and these reported links between liver disease and both intestinal dysbiosis and bacterial/bacterial product translocation, we hypothesized that intestinal IL-17R signaling may play a critical role in mitigating hepatic inflammation.

To test this, we used intestinal epithelium-specific IL-17RA knockout mice (*Il17ra*$^{fl/fl}$ × *villin cre*$^{+}$ mice) in the concanavalin A (Con A) model of T cell-mediated hepatitis. Absence of enteric IL-17RA signaling induced commensal dysbiosis, expansion of intestinal Th17 cells, and intestinal *Il18* expression. After Con A administration, *Il17ra*$^{fl/fl}$ × *villin cre*$^{+}$ mice exhibited more severe hepatitis and increased hepatocyte cell death. Mechanistically, disease exacerbation was microbiome-dependent and associated with gram-negative bacteria. In addition, intestinal-specific knockout mice displayed increased translocation of unmethylated CpG DNA to the liver. Our data suggested that CpG DNA exacerbates liver inflammation by driving expression of hepatic IL-18 to promote interferon gamma (IFNγ) and FasL production in hepatic T cells. Thus, intestinal IL-17R regulates translocation of TLR9 ligands and constrains susceptibility to hepatic inflammation. Our studies elucidate the role of enteric Th17 signaling and the microbiome in hepatitis, with broader implications on the effects of impaired intestinal immunity and subsequent release of microbial products seen in other diseases.

RESULTS

Deletion of IL-17RA in Intestinal Epithelium Exacerbates Concanavalin A Hepatitis

To investigate how intestinal IL-17 signaling regulates liver inflammation, we treated *Il17ra*$^{fl/fl}$ × *villin cre*$^{+}$ mice with intravenous Con A, a plant lectin, to induce a T cell-dependent liver injury (Tiegs et al., 1992). We have previously shown that globally deleting *Il17ra* is protective in this model of hepatitis (Nagata et al., 2008). Interestingly, deleting *Il17ra* signaling specifically in the intestinal epithelium exacerbated disease (Figure 1). As compared to littermate *Il17ra*$^{fl/fl}$ controls, *Il17ra*$^{fl/fl}$ × *villin cre*$^{+}$ mice exhibited elevated serum alanine aminotransferase (ALT), a marker of liver inflammation, and increased mortality rates (Figures 1A and 1B). Liver pathology revealed substantially larger patches of cell death in the hepatic parenchyma (Figure 1C). Indeed, quantification of cell death by TUNEL staining showed ~50% more cell death on average in *Il17ra*$^{fl/fl}$ × *villin cre*$^{+}$ mice as compared to littermate floxed controls (Figure 1D).

Exacerbated Liver Injury Is Dependent on the Intestinal Microbiota

Given the role of Th17 cells in regulating the intestinal microbiota (Blaschitz and Raffatellu, 2010; Ivanov et al., 2009; Kumar et al., 2016), we tested whether the exacerbated liver injury was microbiome-dependent. Littermate *Il17ra*$^{fl/fl}$ × *villin cre*$^{+}$ mice and *Il17ra*$^{fl/fl}$ controls were either cohoused or separated by genotype for 1 week prior to Con A injection. When separated, knockouts continued to demonstrate more severe disease as measured by ALT (Figure 2A). Cohousing the groups to share the intestinal microbiota between mice eliminated significant differences in ALT levels (Figure 2B), suggesting that disease exacerbation is microbiome-dependent.

IL-17 has been strongly implicated in the regulation of bacteria in the small intestine, particularly those closely related to the intestinal epithelium such as SFB (Ivanov et al., 2009; Kumar et al., 2016). To that end, we performed 16S rRNA gene sequencing on the small intestine terminal ileum of littermate *Il17ra*$^{fl/fl}$ × *villin cre*$^{+}$ mice and floxed controls to examine changes in the microbiome due to IL-17R deficiency (Figure 2C). An outgrowth of SFB in *Il17ra*$^{fl/fl}$ × *villin cre*$^{+}$ mice was observed in the naive state and became more pronounced after Con A (Figure 2C). There was also an outgrowth of *Enterobacteriaceae* in some *Il17ra*$^{fl/fl}$ × *villin cre*$^{+}$ mice after Con A (Figure 2C). To broadly assess which bacteria may be contributing to liver disease, we treated mice with 2 different antibiotic regimens prior to Con A. Mice either received neomycin to largely target gram-negative bacteria or vancomycin to target SFB and other gram-positive bacteria. Based on ALT, neomycin protected mice while vancomycin had no effect, suggesting gram-negative bacteria contribute to hepatitis in this model (Figures 2D and 2E).

To characterize this further, we considered how the mechanisms by which Th17 cells regulate the microbiome are not necessarily specific to one bacterium but can affect the bacteria that generally reside close to the intestinal epithelium. Therefore, we hypothesized that there was a broad bacterial overgrowth in the gut-specific knockout mice potentially contributing to disease. Flow cytometry partnered with counting beads (Gopalakrishna et al., 2019; Palm et al., 2014; Vandeputte et al., 2017) showed increased fecal bacterial burden in

Il17ra$^{fl/fl}$ × *villin cre*$^{+}$ mice as compared to littermate floxed controls (Figure S1A). Because transcytosis of intestinal secretory IgA is regulated by IL-17RA, IgA binding on bacteria was analyzed. *Il17ra*$^{fl/fl}$ × *villin cre*$^{+}$ mice had a substantial enrichment for IgA unbound (IgA^{-}) bacteria (Figures S1B and S1C). Both the general bacterial overgrowth and elevated IgA^{-} bacteria were depleted with neomycin (Figures S1A–S1C), suggesting that the bacteria involved in disease exacerbation were IgA^{-} bacteria overgrowing in the intestine in the absence of intestinal IL-17 regulation.

Next, we sought to assess how the *Il17ra*$^{fl/fl}$ × *villin cre*$^{+}$ microbiota was influencing liver disease. Because Th17 signaling is critical for mucosal barrier integrity (Blaschitz and Raffatellu, 2010; Lee et al., 2015; Shih et al., 2014), and intestinal blood drains through the portal system to the liver, it is possible that bacteria were physically translocating to the liver. Initial assessment by 16S qRT-PCR on the livers of naive *Il17ra*$^{fl/fl}$ × *villin cre*$^{+}$ mice and littermate controls showed an increased 16S rRNA gene signal in gut-specific knockout mice (Figure 2F), suggesting more bacteria or bacterial products in the liver of these mice at baseline. We were unable to grow live bacteria from the liver in both aerobic and anaerobic conditions (data not shown) and therefore used mouse TLR (mTLR) reporter cell lines to assay for bacterial products. With a focus on gram-negative bacteria, serum and liver homogenate from naive *Il17ra*$^{fl/fl}$ × *villin cre*$^{+}$ mice and littermate controls were plated on mTLR4 or mTLR9 reporter cells to measure lipopolysaccharide (LPS) and unmethylated CpG DNA levels, respectively. There were no differences in LPS levels in the serum or liver (Figures S1D and S1E). However, there was elevated CpG DNA in the liver of *Il17ra*$^{fl/fl}$ × *villin cre*$^{+}$ mice as measured by the mTLR9 reporter line (Figure 2G). In addition, we found that the CpG DNA signal in the liver was not sensitive to DNase treatment (Figure S1F), potentially implicating a role for microvesicle transport of CpG. Elevated CpG DNA was not seen in serum (Figure 2H), suggesting both that the liver is successfully filtering products from entering the circulation, and CpG DNA may be signaling through TLR9 locally in the liver to influence disease. The presence of increased bacterial products without detectable live bacteria is consistent with the lack of an intestinal barrier defect in *Il17ra*$^{fl/fl}$ × *villin cre*$^{+}$ as measured by fluorescein isothiocyanate (FITC) dextran (Figure S1G), although the possibility of unculturable bacteria translocating to the liver cannot be ruled out. To model if elevated CpG DNA prior to disease induction exacerbates disease, wild-type *C57BL/6* mice were treated with 3 doses of CpG DNA a week prior to Con A (Figure S1H). CpG DNA administration prior to Con A dramatically increased mortality rates as compared to Con A, CpG DNA, or vehicle control alone (Figure S1I).

Intestinal IL-17RA Constrains TLR9-Induced Type I Immune Responses in the Liver

CpG DNA and subsequent TLR9 signaling are capable of eliciting a variety of inflammatory cytokines such as IL-12, IL-6, and interferons (Gupta et al., 2006; Hartmann et al., 1999; Yi et al., 1996). To investigate which CpG-inducible cytokines may be contributing to worsened liver disease, we first wanted to establish which cytokines were elevated in *Il17ra*$^{fl/fl}$ × *villin cre*$^{+}$ mice. To employ a broad, unbiased approach, we performed single-cell RNA (scRNA) sequencing. Previous reports detailed cytokine changes at the protein level within hours of Con A injection (Wang et al., 2012). Therefore, we chose a 90-min post-injection time point to investigate transcriptional changes induced early in the model. We compared the liver

transcriptome of *Il17ra*$^{fl/fl}$ × *villin cre*$^{+}$ mice against littermate *Il17ra*$^{fl/fl}$ controls. Based on dimensionality reduction and upregulation of cell-specific genes (Table S1), we identified 12 distinct cell populations (Figure 3A). Across many cell populations, *Ifng* was one of the significantly upregulated genes in *Il17ra*$^{fl/fl}$ × *villin cre*$^{+}$ mice (Figures 3B and 3C), while liver IL-17, other T helper cytokines, and various cytokines previously implicated in Con A were not significantly different (Figure S2). IFNγ is a known contributor to liver inflammation in Con A hepatitis and an indicator of lymphocyte activation (Mizuhara et al., 1996; Nishikage et al., 1999; Tagawa et al., 1997). In the scRNA sequencing dataset, *Ifng* was expressed by natural killer (NK) cells and CD4, CD8, and NK T cells (Figures 3A and 3C). Downstream IFNγ targets such as *Cxcl9* and *Cxcl10* were also increased (Figure 3B), providing further evidence of *Ifng* upregulation.

To confirm this at the protein level, we performed flow cytometry at the naive state and 5 h post-Con A injection (Figures 3D and 3E). There were more IFNγ^{+} cells in the liver of *Il17ra*$^{fl/fl}$ × *villin cre*$^{+}$ mice after Con A as compared to littermate controls (Figures 3D and 3E). This was due to significant increases in IFNγ-producing T-cell receptor β^{-} (TCRβ^{-}) cells, namely NK cells (Figure 3E). Although there were no differences in the %IFNγ^{+} cells, *Il17ra*$^{fl/fl}$ × *villin cre*$^{+}$ mice displayed an increase in actual IFNγ^{+} cell number due to a 25%–30% increase in liver cellularity observed both at the naive state and 5 h post-Con A (Figure 3F). These differences were not observed in cohoused mice, suggesting these changes were microbiome-dependent (Figures S3A–S3E).

To confirm that CpG DNA can induce liver IFNγ, liver mononuclear cells from naive wild-type *C57BL/6* mice were stimulated with increasing concentrations of CpG DNA or other TLR ligands. To assess whether these ligands can synergize with Con A, each TLR ligand was tested with or without Con A. CpG DNA, LPS, and lipoteichoic acid, a TLR2 ligand, all induced IFNγ responses (Figure 3G). In contrast, flagellin, a TLR5 ligand, did not induce IFNγ responses (Figure 3G). Even at low concentrations, CpG DNA induced strong IFNγ responses both in the absence and presence of Con A (Figure 3G). These data confirmed that CpG DNA is a potent inducer of IFNγ and suggested that CpG DNA may not only contribute to the elevated IFNγ observed in *Il17ra*$^{fl/fl}$ × *villin cre*$^{+}$ mice but also synergize with Con A *in vivo* to enhance responses and worsen disease.

To assess differences in CpG-induced IFNγ responses and determine the cellular source of IFNγ, liver mononuclear cells from *Il17ra*$^{fl/fl}$ × *villin cre*$^{+}$ mice and littermate controls were stimulated with CpG DNA *ex vivo*. By flow cytometry, there was already a slight increase in IFNγ^{+} cells in *Il17ra*$^{fl/fl}$ × *villin cre*$^{+}$ liver cells cultured in media alone (Figures 3H and 3I). This supported our hypothesis that the elevated CpG DNA at baseline may be inducing inflammatory cytokines locally. After CpG DNA treatment, the elevated IFNγ became more pronounced (Figure 3I). Much of the IFNγ came from CD4^{+} and CD8^{+} T cells (Figures 3I and S3F), although knockout mice only demonstrated significantly increased CD8^{+} IFNγ producers (Figure 3I). Taken together, these data suggest that in addition to having more CpG DNA in their livers at baseline, intestinal-specific knockouts demonstrate a baseline low-level elevation in IFNγ and enhanced responses to CpG DNA. This prompted the question of what factors were present in *Il17ra*$^{fl/fl}$ × *villin cre*$^{+}$ mice that were responsible for enhancing IFNγ responses. In addition, TLR9 is not highly expressed on T or NK cells,

potentially implicating an intermediate factor both *in vivo* and *ex vivo* to facilitate these IFNγ responses to CpG DNA.

Intestinal IL-17RA Constrains Hepatic and Intestinal IL-18

scRNA sequencing also revealed increased *Il18* in *Il17ra*$^{fl/fl}$ × *villin cre*$^{+}$ livers (Figures 4A and 4B). IL-18 has been implicated in many inflammatory conditions such as macrophage activation syndrome, rheumatoid arthritis, and hepatitis (Kaplanski, 2018; Morel et al., 2001; Weiss et al., 2018). We chose to investigate IL-18 further due to its established ability to enhance IFNγ production (Kaplanski, 2018; Nakamura et al., 1993).

Within the liver, bacterial products like CpG DNA have been shown to activate cells close to the hepatic vasculature, such as Kupffer cells (KCs) and hepatic stellate cells (Carpino et al., 2004; Dobashi et al., 1999; Fujita et al., 2016; Seki et al., 2001; Szabo et al., 2010). Indeed, analysis of the scRNA sequencing data showed that *Il18* was expressed mainly in KCs, cholangiocytes, and to a lesser extent, a non-KC monocyte/macrophage population (Figure 4A). Consistent with the scRNA sequencing data, IL-18 was increased by transcript in the liver and protein in liver and serum of naive *Il17ra*$^{fl/fl}$ × *villin cre*$^{+}$ mice (Figures 4C–4E). Furthermore, differences in IL-18 in the liver and serum were not observed in cohoused littermate naive *Il17ra*$^{fl/fl}$ and *Il17ra*$^{fl/fl}$ × *villin cre*$^{+}$ mice, suggesting the differences in IL-18 are microbiome-dependent (Figures S4A and S4B).

We also observed elevated *Il18* in the small intestine of *Il17ra*$^{fl/fl}$ × *villin cre*$^{+}$ mice (Figure 4F), suggesting that in addition to local sources, the elevated liver IL-18 may also be coming from the intestine through the portal circulation. Furthermore, neomycin treatment in the drinking water (that depletes gram-negative bacteria) decreased serum IL-18, providing additional support for not just intestinal involvement, but specifically microbiome involvement in IL-18 regulation (Figure 4G). To further assess the potential contribution of intestinal IL-18 in disease exacerbation, *Nlrc4*^{mut}*Il18bp*$^{-/-}$ mice were treated with Con A. In these mice, IL-18 binding protein (IL-18BP), which is necessary for regulatory inhibition of IL-18, is knocked out, and the NLRC4 T337S mutation causes excess inflammasome-mediated IL-18 from the intestine (Weiss et al., 2018). After administration of Con A, these mice exhibited lethal hepatitis, while single mutant and wild-type controls survived (Figure S4C). This suggested that excess intestinal IL-18 partnered with decreased systemic inhibition of IL-18 promotes hepatitis and implies a pathogenic role for excess intestinal IL-18 in *Il17ra*$^{fl/fl}$ × *villin cre*$^{+}$ mice.

To assess whether CpG DNA plays a role in the elevated hepatic IL-18 levels, hepatic mononuclear cells were stimulated *ex vivo* with CpG DNA. Indeed, we observed IL-18 induction after CpG DNA stimulation (Figure 4H). Moreover, CpG-induced IFNγ was decreased *ex vivo* by treatment with anti-IL-18, suggesting that CpG DNA is inducing liver IFNγ in an IL-18-dependent manner (Figure 4I). To assess the functional role of IFNγ on exacerbated disease, *Il17ra*$^{fl/fl}$ × *villin cre*$^{+}$ mice were treated with anti-IFNγ prior to Con A injection. Interestingly, IFNγ blockade did not ameliorate disease (Figure S4D) despite confirmation of IFNγ neutralization by serum ELISA (Figure S4E). Because of this, we examined other downstream IL-18 targets that may be contributing to disease.

IL-18 is a pleiotropic cytokine. Beyond its ability to induce IFNγ, its range of functions include changing cell activation molecules, chemokine production, and *Fasl* expression (Kaplanski, 2018; Tsutsui et al., 1999, 2000). We observed changes in gene expression consistent with IL-18 effects described in the literature (Bachmann et al., 2018; Enoksson et al., 2011; Gutzmer et al., 2003; Kang et al., 2007; Kojima et al., 1999; Okamoto et al., 1999; Sattler et al., 2015; Subleski et al., 2007; Tsutsui et al., 1996; Weinstock et al., 2003; Yoo et al., 2005). Many of these changes were observed soon after Con A injection rather than at the naive state (Figure S5), suggesting a requirement for additional stimulation. This supports IL-18's function as an amplifier of other cytokines (Dinarello et al., 2013). 90 min after Con A injection, there were markers of increased activation, chemokine expression, and effector function in the livers of *Il17ra*$^{fl/fl}$ × villin cre mice (Figure 4J). Changes in these downstream *Il18* targets may also be playing a role in liver pathology.

IL-18-Induced FasL Exacerbates Liver Inflammation

Among downstream IL-18 targets, Fas ligand (FasL) in particular, has been strongly implicated in Con A hepatitis, as knockout of either *Fas* or *Fasl* is sufficient to ameliorate disease (Seino et al., 1997; Tagawa et al., 1998; Tsutsui et al., 1999). Within the liver, *Fasl* was mainly expressed by T cells, NK cells, and NKT cells (Figure 5A). We observed increased FasL+ cells and FasL geometric mean fluorescence intensity in the liver of naive *Il17ra*$^{fl/fl}$ × *villin cre*$^{+}$ mice by flow cytometry (Figures 5B–5D). These differences were eliminated upon cohousing, suggesting these FasL changes were microbiome-dependent (Figure S6).

To test the functional role of FasL in disease exacerbation, we treated mice with anti-FasL 1 h prior to Con A injection. Anti-FasL treatment ameliorated hepatitis in gut-specific knockout mice to disease severity comparable to controls based on serum ALT and TUNEL staining (Figures 5E–5G). To investigate whether IL-18 can induce liver FasL, liver mononuclear cells were stimulated *ex vivo* with IL-18 ± anti-IFNγ and analyzed by flow cytometry (Figures 5H and 5I). While there were no significant differences between responses of naive knockouts and controls, results showed that IL-18 stimulated FasL production in TCRβ^{+} cells in an IFNγ-independent manner (Figures 5H and 5I), consistent with the inability of IFNγ blockade to temper exaggerated Con A hepatitis.

Anti-IL18 Mitigates Liver Injury in Intestinal IL-17RA-Deficient Mice

Finally, to assess whether the elevated IL-18 in *Il17ra*$^{fl/fl}$ × *villin cre*$^{+}$ mice was contributing to worsened liver disease, we treated *Il17ra*$^{fl/fl}$ × *villin cre*$^{+}$ mice and littermate controls with anti-IL-18 or isotype control 1 day prior to Con A injection. Anti-IL-18 treatment decreased hepatitis, as measured by serum ALT, in *Il17ra*$^{fl/fl}$ × *villin cre*$^{+}$ mice to levels comparable to wild-type mice (Figure 6A). Liver pathology correspondingly showed reduced areas of cell death in the liver parenchyma (Figures 6B and 6C). Quantification of TUNEL staining confirmed that cell death in *Il17ra*$^{fl/fl}$ × *villin cre*$^{+}$ mice was substantially reduced to levels comparable to littermate floxed controls (Figure 6B). Furthermore, anti-IL-18 treatment reduced liver *Ifng* and *Fasl* transcript in *Il17ra*$^{fl/fl}$ × *villin cre*$^{+}$ mice 8 h post-Con A as measured by qRT-PCR (Figures 6D and 6E).

DISCUSSION

Our results provide evidence that perturbation of intestinal IL-17 signaling is sufficient to exacerbate liver inflammation. Abrogation of intestinal IL-17RA disrupted the intestinal microbiota and promoted translocation of bacterial products to the liver. Together, this induced IL-18 production and subsequent lymphocyte activation and cell death to worsen hepatitis.

Numerous studies have implicated Th17 cells in liver inflammation. For example, both autoimmune hepatitis (AIH) and viral hepatitis patients display elevated serum IL-17 (Shin et al., 2016; Ye et al., 2010; Zhao et al., 2011). In Con A hepatitis, our lab previously showed that *Il17ra*$^{-/-}$ mice were protected from disease (Nagata et al., 2008). However, the role of Th17 cells in liver disease is complex. Here, by using intestinal epithelium-specific knockout mice, we uncouple intestinal IL-17 signaling from systemic signaling to reveal a protective role of intestinal IL-17RA in mitigating liver inflammation. *Il17ra*$^{fl/fl}$ × *villin cre*$^{+}$ mice do have elevations in serum IL-17A (Kumar et al., 2016) capable of mediating systemic effects. However, there are conflicting reports about the role of systemic IL-17 in Con A hepatitis (Lafdil et al., 2009; Nagata et al., 2008; Yan et al., 2012; Zenewicz et al., 2007) that we would hypothesize are due to institutional differences in the microbiome or the contribution of other IL-17RA cytokines. This negative contribution of intestinal IL-17 relative to systemic IL-17 paralleled findings in the experimental autoimmune encephalomyelitis (EAE) mouse model of multiple sclerosis. In EAE, global IL-17RA deficiency was protective (Gonzalez-García et al., 2009), while intestinal specific deficiency was detrimental (Kumar et al., 2016), indicating that intestinal IL-17 signaling and potentially control over the microbiota can have wide-ranging effects that are amplified by IL-17 signaling outside the intestine.

While reports have separately associated Th17 cells and the microbiome to liver inflammation, our study adds to the existing literature by linking these factors together in the context of liver disease (Boursier and Diehl, 2015; Chen et al., 2014; Lafdil et al., 2010; Leung and Yimlamai, 2017). Although IL-17 from multiple cellular sources (i.e., CD4 T cells, ILCs, and γδ T cells) can affect liver injury, our data suggest there is no increase in liver IL-17 within *Il17ra*$^{fl/fl}$ × *villin cre*$^{+}$ mice. Therefore, rather than IL-17 acting locally in the liver, our data suggest that disruption of intestinal IL-17RA promoted intestinal overgrowth of gram-negative, IgA^{-} bacteria that exacerbated liver inflammation. The presence of gram-negative bacteria exacerbating liver inflammation corroborates previous studies showing that germfree mice and mice treated with gentamicin are protected in Con A hepatitis (Celaj et al., 2014; Chen et al., 2014). Moreover, IgA has been previously shown to skew toward binding molecules such as flagellin and fimbriae that are important for association with the intestinal epithelium (Cullender et al., 2013). Thus, an increase in IgA^{-} bacteria could be associated with greater bacterial residence adjacent to the enterocytes. At the naive state, 16S data mainly showed differences in SFB. However, vancomycin treatment eliminated SFB and other gram-positive bacteria but had no effect on Con A hepatitis, suggesting that SFB are not detrimental in this model. This is consistent with data showing that SFB^{-} Jackson Laboratories wild-type mice had worse Con A hepatitis than SFB^{+} Taconic wild-type mice (Celaj et al., 2014). After Con A, *Il17ra*$^{fl/fl}$ × *villin cre*$^{+}$ mice

displayed a bloom of *Enterobacteriaceae,* which have particularly stimulatory CpG DNA (Bouladoux et al., 2012). However, this overgrowth may simply be a consequence of inflammation as *Enterobacteriaceae* are known to outcompete other bacteria and bloom in inflammatory environments (Winter and Bäumler, 2014). It is also possible that we were not able to observe other changes by 16S, because an intrinsic limitation of this assay is that it does not take into account absolute bacteria counts. Therefore, the general structure of the microbiota may not appear to be changed by relative abundance of specific bacterial taxa, but changes in bacterial behavior as well as absolute amount of bacteria may contribute to disease.

In addition to alterations in the intestinal microbiome, other groups have observed increased bacterial translocation in both patients with and mouse models of liver inflammation (Chen et al., 2014; Lin et al., 2015; Pan et al., 2012). However, the downstream effects on local hepatic immune cell populations remain unclear. Here, we show that at the naive state, disruption of intestinal IL-17R signaling was sufficient to increase flux of bacterial products, specifically CpG DNA, into the liver despite no detectable functional manifestation of intestinal barrier defect. This elevated CpG DNA signal in the liver was not sensitive to DNase treatment, raising the possibility of CpG DNA transport into the liver via outer membrane vesicle (OMV) release. This aligns with our data implicating gram-negative bacteria in our model, as gram-negative bacteria have been shown to produce OMVs (Schwechheimer and Kuehn, 2015). Our data and a study by Jiang et al. (2009) both demonstrated that CpG DNA worsened Con A hepatitis. There was a conflicting report detailing hepatitis attenuation after CpG DNA stimulation (Zhang et al., 2010), but we postulate this is due to differences in the CpG DNA and treatment regimen used in the experiments. In our study, we showed that CpG DNA induced IL-18-dependent liver IFNγ production from T cells, providing evidence that intestinal IL-17 signaling may play a role in constraining TLR9 induced-Type I liver responses.

Il17ra$^{fl/fl}$ × *villin cre*$^{+}$ mice also exhibited increased intestinal *Il18*. Our data showing exacerbated hepatitis in *Nlrc4*^{mut}*Il18bp*$^{-/-}$ mice suggest a pathogenic role for excess intestinal IL-18. In addition, elevated intestinal IL-18 within *Il17ra*$^{fl/fl}$ × *villin cre*$^{+}$ mice is consistent with previous reports that IL-18 is produced by intestinal epithelial cells in response to IL-22 (Muñoz et al., 2015). Indeed, we have previously shown that disrupted intestinal IL-17RA signaling increased intestinal IL-22^{+} cells and downstream AMPs such as *Reg3g* (Kumar et al., 2016). Increased IL-22-driven production of AMPs may neutralize the highly toxic LPS and explain why gram-negative bacteria are implicated in disease with quantifiable differences in CpG DNA but not LPS. Interestingly, serum IL-18 was partially decreased with neomycin treatment. Therefore, in addition to intestinal IL-22 regulation of IL-18, intestinal IL-17 signaling may regulate IL-18 through the microbiota. Here, we provided evidence that bacterial products, specifically CpG DNA, induce liver IL-18 within our model. The microbiome may also influence IL-18 levels indirectly through bacterial metabolites (Levy et al., 2015; Nowarski et al., 2015), cytokines (Muñoz et al., 2015), or the inflammasome (Elinav et al., 2011). In concert with these findings, our data imply that perturbations in the microbiome and/or translocation of microbial products can enhance systemic IL-18 levels and affect extra-intestinal pathologies.

Excess IL-18 in *Il17ra*$^{fl/fl}$ × *villin cre*$^{+}$ mice also induced liver FasL, increasing cell death and worsening hepatitis. This is consistent with reports implicating Fas-FasL in Con A hepatitis. Indeed, knockout of either Fas or FasL ameliorated disease within this model (Seino et al., 1997; Tagawa et al., 1998; Tsutsui et al., 1999). In other model systems such as acetaminophen-induced liver injury, IL-18 has also been shown to induce *Fasl* expression (Bachmann et al., 2018; Faggioni et al., 2001; Tsutsui et al., 1996). Here, we demonstrated that IL-18 induced FasL in an IFNγ-independent manner. Therefore, while IL-18 is able to independently induce FasL and IFNγ, our data suggest that the elevated IFNγ in *Il17ra*$^{fl/fl}$ × *villin cre*$^{+}$ mice was more a reflection of increased lymphocyte activation, and FasL was the major IL-18-downstream contributor to disease exacerbation. In addition, the absence of biological or statistical differences in liver inflammation between the knockouts and controls treated with anti-IL-18 demonstrated that anti-IL-18 reduced disease in the knockout mice to levels comparable to that of controls. The lack of protection conferred to control mice suggests that IL-18 is not necessary for disease induction, but rather sufficient in excess for disease exacerbation as demonstrated in the knockout mice. Beyond our model, we established a connection between intestinal IL-17 signaling and hepatic FasL through IL-18, potentially implicating intestinal IL-17 in the many liver diseases linked to Fas-FasL-associated cell death including fulminant, alcoholic, and viral hepatitis as well as liver carcinoma and fibrosis (Guicciardi and Gores, 2006; Hammam et al., 2012; Pinkoski et al., 2000; Tagami et al., 2003).

Despite Con A inducing T cell-mediated hepatitis in the absence of viral infection or autoantibodies, the data within the literature suggest our work is consistent with observations in human disease. For example, AIH patients exhibit increased IFNγ and Fas in bone marrow mononuclear cells (Tsikrikoni et al., 2005), Fas/FasL in liver tissue, and peripheral blood lymphocytes (Fox et al., 2001; Ogawa et al., 2000) compared to healthy controls. Furthermore, IFNγ in liver biopsies (Hussain et al., 1994) and serum IL-18 (Yamano et al., 2000) were both elevated and correlated with disease severity. In chronic hepatitis C, hepatic levels of IFNγ-inducible chemokines including CXCL9 and CXCL10 (Zeremski et al., 2008) and serum IL-18 (Sharma et al., 2009) were elevated and correlated with severity of liver damage. In fulminant hepatitis, there were increased circulating IFNγ^{+} CD8 T cells (Kimura et al., 1999) and serum IL-18 (Shinoda et al., 2006). Furthermore, a recently published report showed that excess IL-18 due to genetic IL-18BP deficiency in human patients can promote fulminant immunopathology during viral hepatitis (Belkaya et al., 2019). As such, we believe the mechanisms described in our work are potentially translatable to clinical hepatitis in patients.

Our data may also have implications on hepatic diseases and illnesses beyond the gut-liver axis in conditions with “leaky gut” and increased bacterial translocation. This study reveals potential immune consequences of the subclinical bacteremia observed in many patients. For example, in HIV/AIDS, much emphasis has been placed on leakage of LPS across the gut barrier causing wasting and chronic inflammation (Brenchley et al., 2006). Our data suggest that extra-intestinal TLR9 ligand dissemination is regulated by intestinal IL-17R signaling and may therefore be another underlying mechanism in HIV/AIDS liver dysfunction (Chamroonkul and Bansal, 2019). Taken together, the connection our data established

between intestinal Th17 cells, the microbiome, and hepatic immune signaling elucidate therapeutic avenues to explore to treat hepatitis and other extra-intestinal diseases.

STAR★METHODS

LEAD CONTACT AND MATERIALS AVAILABILITY

Further information and requests for resources and reagents should be directed to and will be fulfilled by the Lead Contact, Jay K. Kolls (jkolls1@tulane.edu). Distribution of the anti-IL-18 reagent is restricted under an MTA with Genentech.

EXPERIMENTAL MODEL AND SUBJECT DETAILS

Mice—All mouse work was performed in accordance with the Institutional Animal Care and Use Committees (IACUC) and relevant guidelines at the University of Pittsburgh, School of Medicine. *C57BL/6* mice were obtained from Taconic Biosciences (Germantown, NY). *Nlrc4*^{mut}, *Il18bp*$^{-/-}$, and *Nlrc4*^{mut}*Il18bp*$^{-/-}$ mice were obtained from Dr. Scott Canna at the UPMC Children's Hospital of Pittsburgh. *Il17ra*$^{fl/fl}$ and *Il17ra*$^{fl/fl}$ × *villin cre*$^{+}$ mice were generated at the UPMC Children's Hospital of Pittsburgh by crossing *Il17ra*$^{fl/fl}$ mice to *Il17ra*$^{fl/fl}$ × *villin cre*$^{+}$ mice. Both male and female age-matched mice from 6–10 weeks of age were used for all experiments. The aforementioned breeding strategy allowed for controls and knockout mice within each experiment to be littermates. Littermate age-matched males and females were randomly assigned to experimental groups. Both males and females were used within each group in order to account for sex-differences while maintaining littermate controls and sufficient n for statistical power. All mice were housed in pathogen-free conditions at the UPMC Children's Hospital of Pittsburgh.

***In vitro* and ex *vivo* cultures—**Mouse TLR9 and TLR4 reporter cells (HEK-blue mTLR9 and HEK-dual mTLR4 reporter cells) were obtained from Invivogen and maintained according to manufacturer's instructions. Sex of both cell lines: female.

Ex vivo stimulation of liver cells: Livers from 6–10-week-old naive *Il17ra*$^{fl/fl}$ mice and *Il17ra*$^{fl/fl}$ × *villin cre*$^{+}$ mice were harvested and enriched for mononuclear cells by Percoll gradient. In addition to detailed experiment-specific stimuli, cells were maintained at 37°C in Iscove's Modified Dulbecco's Medium (IMDM) with GlutaMAX Supplement (GIBCO), 10% heat-inactivated fetal bovine serum, 100 units/mL of penicillin and streptomycin, and 0.3mg/mL of L-glutamine.

Experimental Models—Concanavalin A (Con A) hepatitis was induced using concanavalin A from *Canavalia ensiformis* (jack bean) type IV (Sigma).

METHOD DETAILS

Animal treatments—*C57BL/6, Il17ra*$^{fl/fl}$, and *Il17ra*$^{fl/fl}$ × *villin cre*$^{+}$ mice were injected with 10mg/kg or 25mg/kg Con A intravenously (IV) via tail vein. For antibiotic studies, mice were treated with either five days of 1g/L neomycin or 14 days of 0.5g/L vancomycin in the drinking water *ad libitum* prior to Con A injection and remained on antibiotics throughout the hepatitis model. For CpG DNA pre-treatments, Class C CpG (Invivogen) was

injected 3× at 2.5mg/kg intraperitoneally (IP) prior to 10mg/kg IV Con A. For IFNγ blockade, anti-IFNγ (BioXCell, Clone XMG1.2) was injected IP at 0.5mg/mouse two hours prior to Con A injection. For FasL inhibition, mice were injected with anti-FasL (BioLegend, Clone MFL3) at 250–500 μg/mouse IV into the retro-orbital sinus one hour prior to 25mg/kg Con A injection. For IL-18 blockade, anti-IL-18 (Genentech) was injected IP at 0.5mg/mouse one day prior to 25mg/kg IV Con A injection.

Alanine aminotransferase quantification—Alanine aminotransferase (ALT) was measured in the serum of mice using the Vitros DT60 II chemistry system (Ortho-Clinical Diagnostics, Inc.) (Zheng et al., 2016) or ALT Activity Assay (Sigma) per manufacturer's instructions. Method of ALT measurement was consistent within experiments.

TUNEL Staining—Liver tissues used for TUNEL staining were immediately fixed in 4% paraformaldehyde for 24–72 hours, washed 3× in PBS, and stored in 70% ethanol prior to paraffin embedding. Following paraffin embedding, slides were stained using the ApopTag® Peroxidase *In Situ* Apoptosis Detection Kit according to manufacturer's instructions.

Cohousing studies—Littermate *Il17ra*$^{fl/fl}$ and *Il17ra*$^{fl/fl}$ × *villin cre*$^{+}$ mice were either kept cohoused or separated for one week prior to Con A injection and remained in assigned housing conditions throughout hepatitis model.

qRT-PCR and RNA Sequencing—Livers and intestines from naive 6-10-week-old littermate *Il17ra*$^{fl/fl}$ and *Il17ra*$^{fl/fl}$ × *villin cre*$^{+}$ mice were homogenized in Trizol buffer (Life Technologies). Total RNA extraction was performed according to Trizol manufacturer's instructions. RNA was transcribed into cDNA using iScript reagent (Bio-RAD) according to manufacturer's instructions.

For qRT-PCR, SYBR Green supermix (Bio-RAD) was used for analysis of small subunit ribosomal RNA gene (16S rRNA) expression. 16S primers included: forward: ACTCCTACGGGAGGCAGCAGT, reverse: ATTACCGCGGCTGCTGGC (Croswell et al., 2009; Kumar et al., 2016; Salzman et al., 2010). SsoFast supermix (Bio-RAD) was used for qRT-PCR analysis with primers for mouse *Hprt* (Integrated DNA Technologies), *Ifng* (Applied Biosystems), and *Fasl* (Applied Biosystems). Expression of all genes was normalized relative to housekeeping gene mouse *Hprt*. Reaction: 95°C for 3 minutes, 49 cycles at 95°C for 10 s (s) and 60°C for 30 s. SYBR Green reactions also had an additional melt curve at the end of the reaction above: 60°C for 5 s with +0.5°C increment every cycle up to 95°C.

Terminal ileum bulk RNA sequencing data was sourced from dataset we previously published (Kumar et al., 2016). See previous manuscript for detailed methods.

Single Cell RNA Sequencing—Livers from 6-week-old littermate *Il17ra*$^{fl/fl}$ and *Il17ra*$^{fl/fl}$ × *villin cre*$^{+}$ mice were harvested at the naive state or ninety minutes post 25mg/kg IV Con A injection. Single cell suspensions were isolated and enriched for mononuclear cells via Percoll gradient. Briefly, livers were collected in IMDM with GlutaMax (GIBCO) supplemented with 10% FBS, penicillin, streptomycin, and L-glutamine ("complete

media"). Livers were minced into small pieces and digested in neat IMDM with 1mg/mL collagenase and 0.2mg/mL DNase at 37°C for 30 minutes with shaking. Cell suspension was further homogenized by flowing through an 18G needle in a 3mL syringe followed by filtering through a 70 μm filter. Following a wash in complete media, mononuclear cells were enriched using a 70%/30% percoll gradient. Cells were washed 2× in complete media and resuspended for downstream applications.

For single cell RNA sequencing library preparation, liver cells were then separated into mini-reaction "partitions" or Gel bead in emulsion (GEM)s formed by oil micro-droplets, each containing a gel bead and a cell, by the Chromium instrument (10X Genomics). The reaction mixture/emulsion with captured and barcoded mRNAs were removed from the Chromium instrument followed by reverse transcription. The cDNA samples were fragmented and amplified per 10X protocol. The libraries were then purified, quantified, and sequenced on an Illumina NextSeq 550. Analysis was performed using the pipeline Cell Ranger developed by 10X Genomics as well as Seurat.

16S rRNA Gene Sequencing—Littermate *Il17ra*$^{fl/fl}$ and *Il17ra*$^{fl/fl}$ × *villin cre*$^{+}$ mice were sacrificed at the naive state or 8 hours post Con A injection. Terminal ileum RNA was isolated using Trizol (Life Technologies) and transcribed to cDNA using the iScript Reverse Transcription Supermix (Bio-rad), both according to manufacturer's instructions. Extracted DNA was PCR amplified using the method/primers of Caporaso et al. (2012) and the Q5 HS High-Fidelity polymerase (NEB). Four microliters of each sample were amplified in a 25 μL PCR reaction with barcoded V4 16S primers. Cycle conditions were 98°C for 30 s, then 25 cycles of 98°C for 10 s, 57°C for 30 s, 72°C for 30 s, with a final extension step of 72°C for 2 min. Reactions were purified with AMPure XP beads (Beckman) at a 0.8:1 ratio (beads:DNA) to remove primer-dimers. Eluted DNA was quantitated on a Qubit fluorimeter (Life Technologies). Sample pooling was performed on ice by combining 20ng of each purified band. For negative controls and poorly performing samples, 20 μL of each sample was used. The sample pool was first purified/concentrated with the MinElute PCR purification kit. Next, two-sided AMPure XP bead purification was used at 0.8:1 (left-side) and 0.61:1 (right-side) ratios to remove small and large contaminants, respectively. A final cleanup in the Purelink PCR Purification Kit (Life Technologies) was performed to insure removal of all AMPure XP beads. The final, purified pool was quantitated in triplicate on the Qubit fluorimeter prior to sequencing.

Sequencing pool preparation was as per Illumina's recommendations, with an added incubation at 95°C for 2 minutes immediately following the initial dilution to 20 picomolar. The pool was then diluted to a final concentration of 6 pM + 15% PhiX control. Paired-end sequencing was done on an Illumina MiSeq platform using a MiSeq Reagent kit v2 (500 cycles).

mTLR reporter assays—For mTLR4 and mTLR9 reporter cell assays, cells were grown and maintained according to manufacturer's instructions (Invivogen). For the assay, cells were stimulated with serum or liver homogenate of naive littermate *Il17ra*$^{fl/fl}$ and *Il17ra*$^{fl/fl}$ × *villin cre*$^{+}$ mice. For the liver homogenate, livers were homogenized in PBS plus protease inhibitor (Roche). BCA Protein Assay (Pierce) was performed according to manufacturer's

instructions to measure total protein concentration. Dilutions were performed in PBS plus protease inhibitor to normalize concentrations between samples prior to reporter assay. SEAP levels were measured using QUANTI-Blue detection media (Invivogen). Assays were conducted according to the manufacturer's instructions.

For DNase treatment of liver homogenate, livers were harvested, homogenized in PBS plus protease inhibitors, and diluted to normalize total protein concentration as described above. An aliquot of liver homogenate was treated with DNase I from bovine pancreas (Sigma) reconstituted in PBS + MgCl to activate enzyme per manufacturer's instructions. Vehicle control treatment was PBS + MgCl without DNase. Liver homogenate plus DNase or vehicle control were incubated at 37°C with shaking for 30 minutes. Digested samples were then plated on mTLR9 reporter cell line as described above. Positive control to ensure DNase treatment efficacy was *E. coli* dsDNA (Invivogen). Negative controls were nuclease free water (Thermo Fisher) and nuclease-resistant Class C CpG (Invivogen).

Flow cytometry—Liver single cell suspensions were isolated and enriched for mononuclear cells from *C57BL/6* mice or littermate *Il17ra*$^{fl/fl}$ and *Il17ra*$^{fl/fl}$ × *villin cre*$^{+}$ mice as described above in *Single Cell RNA Sequencing*. For staining, cells were washed in HBSS. Surface and live/dead stains were performed in 50 μl-75 μL in a 96 well round bottom plate in the dark on ice for 20 minutes. Cells were washed 2.5× in cold FACS Buffer (0.5% FBS/0.01% NaN3/PBS). Cells were then fixed using BD Cyto-fix and incubated in the dark on ice for 20 minutes. If no further staining was required, cells were washed 2× in FACS buffer, resuspended in PBS or FACS buffer, and analyzed using the BD Fortessa flow cytometer. If additional intracellular stain analysis was required, cells were washed 1× in BD Perm/Wash. 50–75 μL of intracellular stain cocktail made in BD Perm/Wash was then added to the cells and incubated in the dark on ice for 45 minutes. Cells were then washed 2× in BD Perm Wash, 1× in FACS buffer, and resuspended in PBS or FACS buffer for analysis on the BD Fortessa flow cytometer. Data analysis was performed on FlowJo. Cell number was quantified using the Nexcelom Cellometer Auto 2000. Flow cytometry antibodies used included: Live/Dead fixable aqua dead cell stain (Invivogen) (1:500 dilution), BV786 Anti-mouse CD4 (BD Clone RM4–5) (1:200 dilution, APC Anti-mouse IFNγ (eBiosciences Clone XMG1.2) (1:200 dilution), APCe780 Anti-mouse TCRβ (BD Clone H57–597) dilution), BV421 Anti-mouse NK1.1 (BD clone PK136) (1:100 dilution), BUV395 Anti-mouse CD3 (BD Clone 145–2C11) (1:200 dilution), PCP-Cy5 Rat-Anti-Mouse CD3 Molecular Complex (BD clone 17A2) (1:200 dilution), BV605 Anti-Mouse CD90.2 (BD clone 30-H12) (1:400 dilution), PE Anti-Mouse FasL (Biolegend Clone MFL3) (1:200 dilution), PE-Cy7 Anti-mouse CD8 (Invitrogen clone eBioH35–7.2) (1:400 dilution), Anti-Mouse CD16/CD32 (eBioscience Clone 93).

Fecal Bacterial Flow Cytometry—Protocol based on previously published works (Gopalakrishna et al., 2019; Palm et al., 2014; Vandeputte et al., 2017). Briefly, fecal matter was collected and weighed. 1ml of sterile PBS was added to the fecal content and homogenized by vortex and pipetting. Stool suspension was then passed through a 40-micron strainer into a 50ml conical tube. 10 μL of stool was added to a round-bottom 96-well plate for IgA staining. Plated stool was washed 2.5× in BAC-FACS buffer (filtered

1%BSA in PBS) at 4000rpm for 5 minutes at 4°C. Stool was then stained in BAC-FACS buffer using Hoechst stain (1:1000 dilution) (Life Technologies), normal rat serum (1:5 dilution) (Thermo Fisher), and anti-mouse IgA PE or isotype control (1:500 dilution) (eBioscience clone mA-6E1). Samples were stained for one hour on ice in the dark and washed 2.5× with 100 μL BAC-FACS buffer. Samples were reconstituted in BAC-FACS buffer, and 10 μL of Accu-Check counting beads (Thermo Fisher) were added to each. Samples were analyzed by flow cytometry on the BD Fortessa cytometer. Bacterial calculations using Accu-Check beads (Thermo Fisher) were done using manufacturer's instructions.

***Ex vivo* TLR ligand stimulation—**Liver single cell suspensions were isolated and enriched for mononuclear cells from *C57BL/6* mice or littermate *Il17ra*$^{fl/fl}$ and *Il17ra*$^{fl/fl}$ × *villin cre*$^{+}$ mice as described above in *Single Cell RNA Sequencing*. Cells were then resuspended in IMDM with GlutaMax (GIBCO) supplemented with 10% FBS, penicillin, streptomycin, and L-glutamine ("complete media") and plated at a concentration of 5×10^5 or 1×10^6 cells per well in a 96-well round bottom plate. Cell number was kept consistent within experiments. Cells were then stimulated with various conditions at 37°C for the detailed incubation times. Lipoteichoic acid, flagellin, lipopolysaccharide, and CpG were all attained from Invivogen and used at 10ng/mL-1 μg/mL or 1 μM-5 μM. Exact concentrations are detailed within each figure. During stimulations with TLR ligands ± Concanavalin A, 5ug/mL of Concanavalin A (Sigma) was used. Supernatants were harvested at 24 hours and analyzed for IFNγ and IL-18 levels by ELISA or Luminex. For downstream flow cytometry analysis, brefeldin A (BD) was added for 3 hours after 4 hours of 1 μM CpG stimulation. Cells were then stained and fixed for flow cytometry analysis as described above in *Flow Cytometry*.

ELISA and Luminex Assays—Cytokines from serum, liver homogenate, and cell culture supernatants were measured using the following ELISA or Luminex kits according to the manufacturer's instructions: Mouse-IFNγ ELISA MAX Kit (BioLegend), MILLIPLEX Mouse Th17 Magnetic Bead Panel (Millipore Sigma), Cytokine & Chemokine 36-Plex Mouse Procarta Plex Panel 1A (Thermo Fisher Scientific-Affymetrix), and IL-18 Mouse ELISA Kit (Invitrogen).

FITC Dextran Assay for Intestinal Permeability—Four hours prior to FITC dextran gavage, water bottles were removed from the mouse cages. FITC-dextran (4kDa, Sigma) was dissolved in PBS at a concentration of 100 mg/ml and administered to each mouse at 44mg/100 g body weight by oral gavage. Mice were euthanized after 4 hours, and blood was collected immediately after via cardiac puncture. Serum was isolated from blood samples. For analysis, serum was diluted with an equal volume of PBS. 100 μL of diluted serum was added to a 96-well microplate in duplicate. Concentration of FITC in serum was determined by florescence spectroscopy. The plate was read at an excitation of 485 nm (20 nm band width) and an emission wavelength of 528 nm (20 nm band width). Serially diluted FITC-dextran (0, 125, 250, 500, 1,000, 2,000, 4,000, 6,000, 8,000 ng/ml) was used as a reference standard to calculate serum concentrations. Serum from mice gavaged with saline instead of FITC-dextran was used to determine background.

QUANTIFICATION AND STATISTICAL ANALYSIS

TUNEL Image Quantification—To quantify TUNEL staining, five images spanning the width of the liver slice were taken at 10× magnification. Images were analyzed using ImageJ. Briefly, images were deconvoluted to isolate and analyze only the TUNEL diaminobenzidine (DAB) staining. A threshold of the TUNEL DAB stain was determined to minimize background staining (i.e., vascular endothelial cells, erythrocytes). Identical threshold was applied to all samples per experiment. Using the “measure” feature on ImageJ, TUNEL+ staining was then quantified as the percent of the total image area that was above the set color threshold. To ensure that focal batches of cell death throughout the liver were accounted for, the % area TUNEL+ of all five images were averaged to determine the % Area TUNEL+ per mouse.

Single Cell RNA Sequencing Analysis—Following sequencing described above, we used Cell Ranger version 2.1.1 (10× Genomics) to process raw sequencing data and Seurat suite version 2.2.1 for downstream analysis. Filtering was performed to remove multiplets and broken cells, and non-relevant sources of variation were regressed out. Variable genes were determined by iterative selection based on the dispersion versus average expression of the gene. For clustering, principal component analysis was performed for dimension reduction. Top 10 principal components (PCs) were selected by using a permutation-based test implemented in Seurat and passed to t-SNE for visualization of clusters.

Bulk Intestinal RNA Sequencing Analysis—Data presented is sourced from the dataset we previously published (Kumar et al., 2016). See previous manuscript for detailed statistical analysis.

16S rRNA Gene Sequencing Analysis—Sequence read quality control and classifications were completed using the Center for Medicine and the Microbiome in-house read processing and classification pipeline. The read processing pipeline applied low complexity filtering (NCBI dustmasker), QV trimming, sequence adaptor trimming and primer trimming modules. Sequences with both forward and reverse read directions passing read processing metrics were assembled using the make.contig command from Mothur (Schloss et al., 2009). Mated reads were further screened to limit overlap mismatch proportion (< 0.2), limit N’s allowed (4), and enforce a minimal overlap of 25bp. Merged sequences were classified with a Mothur-dependent in-house pipeline that combines OTU generation and taxonomic classifications using the RDP/Silva classifier and includes chimera screening, clustering and taxonomic classification. The sample taxonomic profile was subsequently represented as a matrix with dimensions: number of samples × number of taxonomic units for compositional analysis with an in-house pipeline which incorporated statistical modules and graphics using the R package (Tarabichi et al., 2015).

Statistical Tests—Statistical tests used are indicated in the figure legends. To compare differences between two groups, student-t test or non-parametric Mann-Whitney test was used depending on the distribution of the data. When comparing one variable in three or more groups, one-way ANOVA with multiple comparisons was used. When comparing multiple variables among two groups, two-way ANOVA with multiple comparisons or

multiple t tests per row was used. GraphPad Prism software was used to analyze experimental groups. For single cell RNA sequencing, statistical analysis was based on the non-parametric Wilcoxon rank sum test. For all data, statistically significant was defined as $p < 0.05$. The degree of statistical significance was defined as: $p < 0.05$*, < 0.01**, < 0.001***, < 0.0001****.

Analysis Software—GraphPad Prism was used for statistical analysis described above. ImageJ was used for histology analysis. Seurat, Cell Ranger, and Loupe Browser were used for single cell RNA sequencing analysis.

DATA AND CODE AVAILABILITY

The accession number for the 16S rRNA sequencing data reported in this paper is SRA BioProject: PRJNA526489. The accession number for the liver single cell RNA sequencing data reported in this paper is GEO: GSE128284 (https://www.ncbi.nlm.nih.gov/geo/query/acc.cgi?acc=GSE128284). The accession number for the original terminal ileum RNA sequencing data (Kumar et al., 2016) is SRA: SRP069071.

Supplementary Material

Refer to Web version on PubMed Central for supplementary material.

ACKNOWLEDGMENTS

We would like to thank Genentech for the anti-IL-18 antibody. We thank Dr. Paul Monga for critical discussion of the project. We thank the U. of Pittsburgh In Situ Hybridization Core for histology assistance. The graphical abstract was created with images adapted from Servier Medical Art by Servier. Original images are licensed under a Creative Commons Attribution 3.0 Unported License (https://creativecommons.org/licenses/by/3.0/legalcode). Research reported in this publication was supported by the National Institute Of General Medical Sciences of the National Institutes of Health (T32GM008208). The authors would also like to acknowledge support from the Richard King Mellon Foundation Institute for Pediatric Research at UPMC Children's Hospital of Pittsburgh and National Heart, Lung, and Blood Institute of the NIH (R35HL13993002 to J.K.K.). P.C.-d.C. was supported by UPMC Children's Hospital of Pittsburgh Research Advisory Committee Grant. The content is solely the responsibility of the authors and does not necessarily represent the official views of the NIH.

REFERENCES

Aly AM, Adel A, El-Gendy AO, Essam TM, and Aziz RK (2016). Gut microbiome alterations in patients with stage 4 hepatitis C. Gut Pathog. 8, 42. [PubMed: 27625705]

Atarashi K, Tanoue T, Ando M, Kamada N, Nagano Y, Narushima S, Suda W, Imaoka A, Setoyama H, Nagamori T, et al. (2015). Th17 cell induction by adhesion of microbes to intestinal epithelial cells. Cell 163, 367–380. [PubMed: 26411289]

Bachmann M, Pfeilschifter J, and Mühl H (2018). A Prominent Role of Interleukin-18 in Acetaminophen-Induced Liver Injury Advocates Its Blockage for Therapy of Hepatic Necroinflammation. Front. Immunol 9, 161. [PubMed: 29472923]

Belkaid Y, and Hand TW (2014). Role of the microbiota in immunity and inflammation. Cell 157, 121–141. [PubMed: 24679531]

Belkaya S, Michailidis E, Korol CB, Kabbani M, Cobat A, Bastard P, Lee YS, Hernandez N, Drutman S, de Jong YP, et al. (2019). Inherited IL-18BP deficiency in human fulminant viral hepatitis. J. Exp. Med 216, 1777–1790. [PubMed: 31213488]

Blaschitz C, and Raffatellu M (2010). Th17 cytokines and the gut mucosal barrier. J. Clin. Immunol. 30, 196–203. [PubMed: 20127275]

Bouladoux N, Hall JA, Grainger JR, dos Santos LM, Kann MG, Nagarajan V, Verthelyi D, and Belkaid Y (2012). Regulatory role of suppressive motifs from commensal DNA. Mucosal Immunol. 5, 623–634. [PubMed: 22617839]

Boursier J, and Diehl AM (2015). Implication of gut microbiota in nonalcoholic fatty liver disease. PLoS Pathog. 11, e1004559. [PubMed: 25625278]

Brenchley JM, Price DA, Schacker TW, Asher TE, Silvestri G, Rao S, Kazzaz Z, Bornstein E, Lambotte O, Altmann D, et al. (2006). Microbial translocation is a cause of systemic immune activation in chronic HIV infection. Nat. Med 12, 1365–1371. [PubMed: 17115046]

Cao AT, Yao S, Gong B, Elson CO, and Cong Y (2012). Th17 cells up-regulate polymeric Ig receptor and intestinal IgA and contribute to intestinal homeostasis. J. Immunol 189, 4666–4673. [PubMed: 22993206]

Caporaso JG, Lauber CL, Walters WA, Berg-Lyons D, Huntley J, Fierer N, Owens SM, Betley J, Fraser L, Bauer M, et al. (2012). Ultra-high-throughput microbial community analysis on the Illumina HiSeq and MiSeq platforms. ISME J. 6, 1621–1624. [PubMed: 22402401]

Carpino G, Franchitto A, Morini S, Corradini SG, Merli M, and Gaudio E (2004). Activated hepatic stellate cells in liver cirrhosis. A morphologic and morphometrical study. Ital. J. Anat. Embryol 109, 225–238. [PubMed: 15717457]

Celaj S, Gleeson MW, Deng J, O'Toole GA, Hampton TH, Toft MF, Morrison HG, Sogin ML, Putra J, Suriawinata AA, and Gorham JD (2014). The microbiota regulates susceptibility to Fas-mediated acute hepatic injury. Lab. Invest 94, 938–949. [PubMed: 25068658]

Chamroonkul N, and Bansal MB (2019). HIV and the liver. Nat. Rev. Gastroenterol. Hepatol 16, 1–2. [PubMed: 30413781]

Chassaing B, Etienne-Mesmin L, and Gewirtz AT (2014). Microbiota-liver axis in hepatic disease. Hepatology 59, 328–339. [PubMed: 23703735]

Chen J, Wei Y, He J, Cui G, Zhu Y, Lu C, Ding Y,Xue R, Bai L, Uede T, et al. (2014). Natural killer T cells play a necessary role in modulating of immune-mediated liver injury by gut microbiota. Sci. Rep 4, 7259. [PubMed: 25435303]

Croswell A, Amir E, Teggatz P, Barman M, and Salzman NH (2009). Prolonged impact of antibiotics on intestinal microbial ecology and susceptibility to enteric Salmonella infection. Infect. Immun 77, 2741–2753. [PubMed: 19380465]

Cullender TC, Chassaing B, Janzon A, Kumar K, Muller CE, Werner JJ, Angenent LT, Bell ME, Hay AG, Peterson DA, et al. (2013). Innate and adaptive immunity interact to quench microbiome flagellar motility in the gut. Cell Host Microbe 14, 571–581. [PubMed: 24237702]

Dinarello CA, Novick D, Kim S, and Kaplanski G (2013). Interleukin-18 and IL-18 binding protein. Front. Immunol 4, 289. [PubMed: 24115947]

Dobashi H, Seki S, Habu Y, Ohkawa T, Takeshita S, Hiraide H, and Sekine I (1999). Activation of mouse liver natural killer cells and NK1.1(+) T cells by bacterial superantigen-primed Kupffer cells. Hepatology 30, 430–436. [PubMed: 10421651]

Elinav E, Strowig T, Kau AL, Henao-Mejia J, Thaiss CA, Booth CJ, Peaper DR, Bertin J, Eisenbarth SC, Gordon JI, and Flavell RA (2011). NLRP6 inflammasome regulates colonic microbial ecology and risk for colitis. Cell 145, 745–757. [PubMed: 21565393]

Enoksson SL, Grasset EK, Hägglöf T, Mattsson N, Kaiser Y, Gabrielsson S, McGaha TL, Scheynius A, and Karlsson MCI (2011). The inflammatory cytokine IL-18 induces self-reactive innate antibody responses regulated by natural killer T cells. Proc. Natl. Acad. Sci. USA 108, E1399–E1407. [PubMed: 22135456]

Faggioni R, Cattley RC, Guo J, Flores S, Brown H, Qi M, Yin S, Hill D, Scully S, Chen C, et al. (2001). IL-18-binding protein protects against lipopolysaccharide-induced lethality and prevents the development of Fas/Fas ligand-mediated models of liver disease in mice. J. Immunol 167, 5913–5920. [PubMed: 11698468]

Fox CK, Furtwaengler A, Nepomuceno RR, Martinez OM, and Krams SM (2001). Apoptotic pathways in primary biliary cirrhosis and autoimmune hepatitis. Liver 21, 272–279. [PubMed: 11454191]

Fujita T, Soontrapa K, Ito Y, Iwaisako K, Moniaga CS, Asagiri M, Majima M, and Narumiya S (2016). Hepatic stellate cells relay inflammation signaling from sinusoids to parenchyma in mouse models of immune-mediated hepatitis. Hepatology 63, 1325–1339. [PubMed: 26248612]

Gonzalez-García I, Zhao Y, Ju S, Gu Q, Liu L, Kolls JK, and Lu B (2009). IL-17 signaling-independent central nervous system autoimmunity is negatively regulated by TGF-beta. J. Immunol. 182, 2665–2671. [PubMed: 19234160]

Gopalakrishna KP, Macadangdang BR, Rogers MB, Tometich JT, Firek BA, Baker R, Ji J, Burr AHP, Ma C, Good M, et al. (2019). Maternal IgA protects against the development of necrotizing enterocolitis in preterm infants. Nat. Med 25, 1110–1115. [PubMed: 31209335]

Guicciardi ME, and Gores GJ (2006). Fasl and fas in liver homeostasis and hepatic injuries. In Fas Signaling H. Wajant, ed. (Springer US), pp. 103–117.

Gupta S, Gould MP, DeVecchio J, Canaday DH, Auletta JJ, and Heinzel FP (2006). CpG-induced IFNgamma expands TLR4-specific IL-18 responses in vivo. Cell. Immunol 243, 75–82. [PubMed: 17292338]

Gutzmer R, Langer K, Mommert S, Wittmann M, Kapp A, and Werfel T (2003). Human dendritic cells express the IL-18R and are chemoattracted to IL-18. J. Immunol 171, 6363–6371. [PubMed: 14662834]

Hammam O, Mahmoud O, Zahran M, Aly S, Hosny K, Helmy A, and Anas A (2012). The role of fas/fas ligand system in the pathogenesis of liver cirrhosis and hepatocellular carcinoma. Hepat. Mon 12, e6132. [PubMed: 23300494]

Hartmann G, Weiner GJ, and Krieg AM (1999). CpG DNA: a potent signal for growth, activation, and maturation of human dendritic cells. Proc. Natl. Acad. Sci. USA 96, 9305–9310. [PubMed: 10430938]

Henao-Mejia J, Elinav E, Thaiss CA, Licona-Limon P, and Flavell RA (2013). Role of the intestinal microbiome in liver disease. J. Autoimmun 46, 66–73. [PubMed: 24075647]

Hussain MJ, Mustafa A, Gallati H, Mowat AP, Mieli-Vergani G, and Vergani D (1994). Cellular expression of tumour necrosis factor-alpha and interferon-gamma in the liver biopsies of children with chronic liver disease. J. Hepatol 21, 816–821. [PubMed: 7534321]

Ivanov II, Atarashi K, Manel N, Brodie EL, Shima T, Karaoz U, Wei D, Goldfarb KC, Santee CA, Lynch SV, et al. (2009). Induction of intestinal Th17 cells by segmented filamentous bacteria. Cell 139, 485–498. [PubMed: 19836068]

Jiang W, Sun R, Zhou R, Wei H, and Tian Z (2009). TLR-9 activation aggravates concanavalin A-induced hepatitis via promoting accumulation and activation of liver CD4+ NKT cells. J. Immunol 182, 3768–3774. [PubMed: 19265155]

Kang M-J, Homer RJ, Gallo A, Lee CG, Crothers KA, Cho SJ, Rochester C, Cain H, Chupp G, Yoon HJ, and Elias JA (2007). IL-18 is induced and IL-18 receptor alpha plays a critical role in the pathogenesis of cigarette smoke-induced pulmonary emphysema and inflammation. J. Immunol 178, 1948–1959. [PubMed: 17237446]

Kaplanski G (2018). Interleukin-18: Biological properties and role in disease pathogenesis. Immunol. Rev 281, 138–153. [PubMed: 29247988]

Kimura K, Ando K, Tomita E, Ohnishi H, Ishikawa T, Kakumu S, Muto Y, and Moriwaki H (1999). Elevated intracellular IFN-γ levels in circulating CD8+ lymphocytes in patients with fulminant hepatitis. J. Hepatol 31, 579–583. [PubMed: 10551378]

Kojima H, Aizawa Y, Yanai Y, Nagaoka K, Takeuchi M, Ohta T, Ikegami H, Ikeda M, and Kurimoto M (1999). An essential role for NF-kappa B in IL-18-induced IFN-gamma expression in KG-1 cells. J. Immunol 162, 5063–5069. [PubMed: 10227974]

Kolls JK, McCray PB Jr., and Chan YR (2008). Cytokine-mediated regulation of antimicrobial proteins. Nat. Rev. Immunol 8, 829–835. [PubMed: 18949018]

Kumar P, Monin L, Castillo P, Elsegeiny W, Horne W, Eddens T, Vikram A, Good M, Schoenborn AA, Bibby K, et al. (2016). Intestinal Interleukin-17 Receptor Signaling Mediates Reciprocal Control of the Gut Microbiota and Autoimmune Inflammation. Immunity 44, 659–671. [PubMed: 26982366]

Lafdil F, Wang H, Park O, Zhang W, Moritoki Y, Yin S, Fu XY, Gershwin ME, Lian Z-X, and Gao B (2009). Myeloid STAT3 inhibits T cell-mediated hepatitis by regulating T helper 1 cytokine and interleukin-17 production. Gastroenterology 137, 2125–2135. [PubMed: 19686746]

Lafdil F, Miller AM, Ki SH, and Gao B (2010). Th17 cells and their associated cytokines in liver diseases. Cell. Mol. Immunol 7, 250–254. [PubMed: 20305686]

Lee JS, Tato CM, Joyce-Shaikh B, Gulen MF, Cayatte C, Chen Y, Blumenschein WM, Judo M, Ayanoglu G, McClanahan TK, et al. (2015). Interleukin-23-Independent IL-17 Production Regulates Intestinal Epithelial Permeability. Immunity 43, 727–738. [PubMed: 26431948]

Leung DH, and Yimlamai D (2017). The intestinal microbiome and paediatric liver disease. Lancet Gastroenterol. Hepatol 2, 446–455. [PubMed: 28497760]

Levy M, Thaiss CA, Zeevi D, Dohnalová L, Zilberman-Schapira G, Mahdi JA, David E, Savidor A, Korem T, Herzig Y, et al. (2015). Microbiota-Modulated Metabolites Shape the Intestinal Microenvironment by Regulating NLRP6 Inflammasome Signaling. Cell 163, 1428–1443. [PubMed: 26638072]

Li W, Amet T, Xing Y, Lan J, Liangpunsakul S, Puri P, Kamath P, Sanyal A, Shah V, Radaeva S, et al. (2017). Enhanced susceptibility to alcohol-induced bacterial translocation, immune activation, and persistent inflammation in patients with alcoholic hepatitis: a prospective observational study. J. Immunol 198 (Suppl 1), 210.9.

Lin R, Zhou L, Zhang J, and Wang B (2015). Abnormal intestinal permeability and microbiota in patients with autoimmune hepatitis. Int. J. Clin. Exp. Pathol 8, 5153–5160. [PubMed: 26191211]

Macpherson AJ, Heikenwalder M, and Ganal-Vonarburg SC (2016). The Liver at the Nexus of Host-Microbial Interactions. Cell Host Microbe 20, 561–571. [PubMed: 27832587]

Mizuhara H, Uno M, Seki N, Yamashita M, Yamaoka M, Ogawa T, Kaneda K, Fujii T, Senoh H, and Fujiwara H (1996). Critical involvement of interferon gamma in the pathogenesis of T-cell activation-associated hepatitis and regulatory mechanisms of interleukin-6 for the manifestations of hepatitis. Hepatology 23, 1608–1615. [PubMed: 8675184]

Morel JC, Park CC, Kumar P, and Koch AE (2001). Interleukin-18 induces rheumatoid arthritis synovial fibroblast CXC chemokine production through NFkappaB activation. Lab. Invest 81, 1371–1383. [PubMed: 11598150]

Muñoz M, Eidenschenk C, Ota N, Wong K, Lohmann U, Kühl AA, Wang X, Manzanillo P, Li Y, Rutz S, et al. (2015). Interleukin-22 induces interleukin-18 expression from epithelial cells during intestinal infection. Immunity 42, 321–331. [PubMed: 25680273]

Nagata T, McKinley L, Peschon JJ, Alcorn JF, Aujla SJ, and Kolls JK (2008). Requirement of IL-17RA in Con A induced hepatitis and negative regulation of IL-17 production in mouse T cells. J. Immunol 181, 7473–7479. [PubMed: 19017936]

Nakamura K, Okamura H, Nagata K, Komatsu T, and Tamura T (1993). Purification of a factor which provides a costimulatory signal for gamma interferon production. Infect. Immun 61, 64–70. [PubMed: 8093360]

Nishikage T, Seki S, Toyabe S, Abo T, Kagata Y, Iwai T, and Hiraide H (1999). Inhibition of concanavalin A-induced hepatic injury of mice by bacterial lipopolysaccharide via the induction of IL-6 and the subsequent reduction of IL-4: the cytokine milieu of concanavalin A hepatitis. J. Hepatol. 31, 18–26. [PubMed: 10424279]

Nowarski R, Jackson R, Gagliani N, de Zoete MR, Palm NW, Bailis W, Low JS, Harman CCD, Graham M, Elinav E, and Flavell RA (2015). Epithelial IL-18 Equilibrium Controls Barrier Function in Colitis. Cell 163, 1444–1456. [PubMed: 26638073]

Ogawa S, Sakaguchi K, Takaki A, Shiraga K, Sawayama T, Mouri H, Miyashita M, Koide N, and Tsuji T (2000). Increase in CD95 (Fas/APO-1)-positive CD4+ and CD8+ T cells in peripheral blood derived from patients with autoimmune hepatitis or chronic hepatitis C with autoimmune phenomena. J. Gastroenterol. Hepatol 15, 69–75. [PubMed: 10719750]

Okamoto I, Kohno K, Tanimoto T, Ikegami H, and Kurimoto M (1999). Development of CD8+ effector T cells is differentially regulated by IL-18 and IL-12.J. Immunol 162, 3202–3211. [PubMed: 10092771]

Palm NW, de Zoete MR, Cullen TW, Barry NA, Stefanowski J, Hao L, Degnan PH, Hu J, Peter I, Zhang W, et al. (2014). Immunoglobulin A coating identifies colitogenic bacteria in inflammatory bowel disease. Cell 158, 1000–1010. [PubMed: 25171403]

Pan C, Gu Y, Zhang W, Zheng Y, Peng L, Deng H, Chen Y, Chen L, Chen S, Zhang M, and Gao Z (2012). Dynamic changes of lipopolysaccharide levels in different phases of acute on chronic hepatitis B liver failure. PLoS ONE 7, e49460. [PubMed: 23185336]

Pinkoski MJ, Brunner T, Green DR, and Lin T (2000). Fas and Fas ligand in gut and liver. Am. J. Physiol. Gastrointest. Liver Physiol 278, G354–G366. [PubMed: 10712254]

Salzman NH, Hung K, Haribhai D, Chu H, Karlsson-Sjöberg J, Amir E, Teggatz P, Barman M, Hayward M, Eastwood D, et al. (2010). Enteric defensins are essential regulators of intestinal microbial ecology. Nat. Immunol 11, 76–83. [PubMed: 19855381]

Sattler A, Dang-Heine C, Reinke P, and Babel N (2015). IL-15 dependent induction of IL-18 secretion as a feedback mechanism controlling human MAIT-cell effector functions. Eur. J. Immunol 45, 2286–2298. [PubMed: 26046663]

Schloss PD, Westcott SL, Ryabin T, Hall JR, Hartmann M, Hollister EB, Lesniewski RA, Oakley BB, Parks DH, Robinson CJ, et al. (2009). Introducing mothur: open-source, platform-independent, community-supported software for describing and comparing microbial communities. Appl. Environ. Microbiol 75, 7537–7541. [PubMed: 19801464]

Schreiber F, Arasteh JM, and Lawley TD (2015). Pathogen Resistance Mediated by IL-22 Signaling at the Epithelial-Microbiota Interface. J. Mol. Biol 427, 3676–3682. [PubMed: 26497621]

Schwechheimer C, and Kuehn MJ (2015). Outer-membrane vesicles from Gram-negative bacteria: biogenesis and functions. Nat. Rev. Microbiol 13, 605–619. [PubMed: 26373371]

Seino K, Kayagaki N, Takeda K, Fukao K, Okumura K, and Yagita H (1997). Contribution of Fas ligand to T cell-mediated hepatic injury in mice. Gastroenterology 113, 1315–1322. [PubMed: 9322527]

Seki E, Tsutsui H, Nakano H, Tsuji N, Hoshino K, Adachi O, Adachi K, Futatsugi S, Kuida K, Takeuchi O, et al. (2001). Lipopolysaccharide-induced IL-18 secretion from murine Kupffer cells independently of myeloid differentiation factor 88 that is critically involved in induction of production of IL-12 and IL-1beta. J. Immunol 166, 2651–2657. [PubMed: 11160328]

Sharma A, Chakraborti A, Das A, Dhiman RK, and Chawla Y (2009). Elevation of interleukin-18 in chronic hepatitis C: implications for hepatitis C virus pathogenesis. Immunology 128 (Suppl 1), e514–e522. [PubMed: 19740312]

Shih VF-S, Cox J, Kljavin NM, Dengler HS, Reichelt M, Kumar P, Rangell L, Kolls JK, Diehl L, Ouyang W, and Ghilardi N (2014). Homeostatic IL-23 receptor signaling limits Th17 response through IL-22-mediated containment of commensal microbiota. Proc. Natl. Acad. Sci. USA 111, 13942–13947. [PubMed: 25201978]

Shin E-C, Sung PS, and Park S-H (2016). Immune responses and immunopathology in acute and chronic viral hepatitis. Nat. Rev. Immunol 16, 509–523. [PubMed: 27374637]

Shinoda M, Wakabayashi G, Shimazu M, Saito H, Hoshino K, Tanabe M, Morikawa Y, Endo S, Ishii H, and Kitajima M (2006). Increased serum and hepatic tissue levels of interleukin-18 in patients with fulminant hepatic failure. J. Gastroenterol. Hepatol 21, 1731–1736. [PubMed: 16984598]

Subleski JJ, Hall VL, Weiss JM, Ortaldo JR, and Wiltrout RH (2007). Differential modulation of NK and NKT cells in the liver and spleen following IL-18 + IL-12 treatment of mice (98.9). J. Immunol 178 (Suppl 1), S193.

Szabo G, Bala S, Petrasek J, and Gattu A (2010). Gut-liver axis and sensing microbes. Dig. Dis 28, 737–744. [PubMed: 21525758]

Tagami A, Ohnishi H, Moriwaki H, Phillips M, and Hughes RD (2003). Fas-mediated apoptosis in acute alcoholic hepatitis. Hepatogastroenterology 50, 443–448. [PubMed: 12749243]

Tagawa Y, Sekikawa K, and Iwakura Y (1997). Suppression of concanavalin A-induced hepatitis in IFN-gamma(−/−) mice, but not in TNF-alpha(−/−) mice: role for IFN-gamma in activating apoptosis of hepatocytes. J. Immunol 159, 1418–1428. [PubMed: 9233639]

Tagawa Y, Kakuta S, and Iwakura Y (1998). Involvement of Fas/Fas ligand system-mediated apoptosis in the development of concanavalin A-induced hepatitis. Eur. J. Immunol 28, 4105–4113. [PubMed: 9862346]

Tarabichi Y, Li K, Hu S, Nguyen C, Wang X, Elashoff D, Saira K, Frank B, Bihan M, Ghedin E, et al. (2015). The administration of intranasal live attenuated influenza vaccine induces changes in the nasal microbiota and nasal epithelium gene expression profiles. Microbiome 3, 74. [PubMed: 26667497]

Tiegs G, Hentschel J, and Wendel A (1992). A T cell-dependent experimental liver injury in mice inducible by concanavalin A. J. Clin. Invest 90, 196–203. [PubMed: 1634608]

Tsikrikoni A, Kyriakou DS, Rigopoulou EI, Alexandrakis MG, Zachou K, Passam F, and Dalekos GN (2005). Markers of cell activation and apoptosis in bone marrow mononuclear cells of patients with autoimmune hepatitis type 1 and primary biliary cirrhosis. J. Hepatol 42, 393–399. [PubMed: 15710223]

Tsutsui H, Nakanishi K, Matsui K, Higashino K, Okamura H, Miyazawa Y, and Kaneda K (1996). IFN-gamma-inducing factor up-regulates Fas ligand-mediated cytotoxic activity of murine natural killer cell clones. J. Immunol 157, 3967–3973. [PubMed: 8892629]

Tsutsui H, Kayagaki N, Kuida K, Nakano H, Hayashi N, Takeda K, Matsui K, Kashiwamura S, Hada T, Akira S, et al. (1999). Caspase-1-independent, Fas/Fas ligand-mediated IL-18 secretion from macrophages causes acute liver injury in mice. Immunity 11, 359–367. [PubMed: 10514014]

Tsutsui H, Matsui K, Okamura H, and Nakanishi K (2000). Pathophysiological roles of interleukin-18 in inflammatory liver diseases. Immunol. Rev 174, 192–209. [PubMed: 10807517]

Vandeputte D, Kathagen G, D'hoe K, Vieira-Silva S, Valles-Colomer M, Sabino J, Wang J, Tito RY, De Commer L, Darzi Y, et al. (2017). Quantitative microbiome profiling links gut community variation to microbial load. Nature 551, 507–511. [PubMed: 29143816]

Wang H-X, Liu M, Weng S-Y, Li J-J, Xie C, He H-L, Guan W, Yuan Y-S, and Gao J (2012). Immune mechanisms of Concanavalin A model of autoimmune hepatitis. World J. Gastroenterol 18, 119–125. [PubMed: 22253517]

Wang Y, Mumm JB, Herbst R, Kolbeck R, and Wang Y (2017). IL-22 Increases Permeability of Intestinal Epithelial Tight Junctions by Enhancing Claudin-2 Expression. J. Immunol 199, 3316–3325. [PubMed: 28939759]

Weinstock JV, Blum A, Metwali A, Elliott D, and Arsenescu R (2003). IL-18 and IL-12 signal through the NF-kappa B pathway to induce NK-1R expression on T cells. J. Immunol 170, 5003–5007. [PubMed: 12734344]

Weiss ES, Girard-Guyonvarc'h C, Holzinger D, de Jesus AA, Tariq Z, Picarsic J, Schiffrin EJ, Foell D, Grom AA, Ammann S, et al. (2018). Interleukin-18 diagnostically distinguishes and pathogenically promotes human and murine macrophage activation syndrome. Blood 131, 1442–1455. [PubMed: 29326099]

Winter SE, and Bäumler AJ (2014). Why related bacterial species bloom simultaneously in the gut: principles underlying the 'Like will to like' concept. Cell. Microbiol. 16, 179–184. [PubMed: 24286560]

Yamano T, Higashi T, Nouso K, Nakatsukasa H, Kariyama K, Yumoto E, Kobayashi Y, Yamamoto K, Iwagaki H, Yagi T, et al. (2000). Serum interferon-gamma-inducing factor/IL-18 levels in primary biliary cirrhosis. Clin. Exp. Immunol 122, 227–231. [PubMed: 11091279]

Yan AW, and Schnabl B (2012). Bacterial translocation and changes in the intestinal microbiome associated with alcoholic liver disease. World J. Hepatol 4, 110–118. [PubMed: 22567183]

Yan S, Wang L, Liu N, Wang Y, and Chu Y (2012). Critical role of interleukin-17/interleukin-17 receptor axis in mediating Con A-induced hepatitis. Immunol. Cell Biol 90, 421–428. [PubMed: 21691280]

Ye Y, Xie X, Yu J, Zhou L, Xie H, Jiang G, Yu X, Zhang W, Wu J, and Zheng S (2010). Involvement of Th17 and Th1 effector responses in patients with Hepatitis B. J. Clin. Immunol 30, 546–555. [PubMed: 20393789]

Yi AK, Chace JH, Cowdery JS, and Krieg AM (1996). IFN-gamma promotes IL-6 and IgM secretion in response to CpG motifs in bacterial DNA and oligodeoxynucleotides. J. Immunol 156, 558–564. [PubMed: 8543806]

Yoo JK, Kwon H, Khil L-Y, Zhang L, Jun H-S, and Yoon J-W (2005). IL-18 induces monocyte chemotactic protein-1 production in macrophages through the phosphatidylinositol 3-kinase/Akt and MEK/ERK1/2 pathways. J. Immunol 175, 8280–8286. [PubMed: 16339568]

Zenewicz LA, Yancopoulos GD, Valenzuela DM, Murphy AJ, Karow M, and Flavell RA (2007). Interleukin-22 but not interleukin-17 provides protection to hepatocytes during acute liver inflammation. Immunity 27, 647–659. [PubMed: 17919941]

Zeremski M, Petrovic LM, Chiriboga L, Brown QB, Yee HT, Kinkhabwala M, Jacobson IM, Dimova R, Markatou M, and Talal AH (2008). Intrahepatic levels of CXCR3-associated chemokines correlate with liver inflammation and fibrosis in chronic hepatitis C. Hepatology 48, 1440–1450. [PubMed: 18798334]

Zhang H, Gong Q, Li JH, Kong XL, Tian L, Duan LH, Tong J, Song FF, Fang M, Zheng F, et al. (2010). CpG ODN pretreatment attenuates concanavalin A-induced hepatitis in mice. Int. Immunopharmacol 10, 79–85. [PubMed: 19818415]

Zhao L,Tang Y, You Z, Wang Q, Liang S, Han X, Qiu D, Wei J, Liu Y, Shen L, et al. (2011). Interleukin-17 contributes to the pathogenesis of autoimmune hepatitis through inducing hepatic interleukin-6 expression. PLoS ONE 6, e18909. [PubMed: 21526159]

Zheng M, Horne W, McAleer JP, Pociask D, Eddens T, Good M, Gao B, and Kolls JK (2016). Therapeutic Role of Interleukin 22 in Experimental Intra-abdominal Klebsiella pneumoniae Infection in Mice. Infect. Immun 84, 782–789. [PubMed: 26729763]

Highlights

- Disruption of intestinal IL-17RA signaling exacerbates immune-mediated hepatitis
- Enhanced disease is microbiome- and IL-18-dependent
- Intestinal IL-17RA constrains translocation of unmethylated CpG DNA to the liver
- Intestinal IL-17RA constrains hepatic FasL and type I responses by regulating IL-18

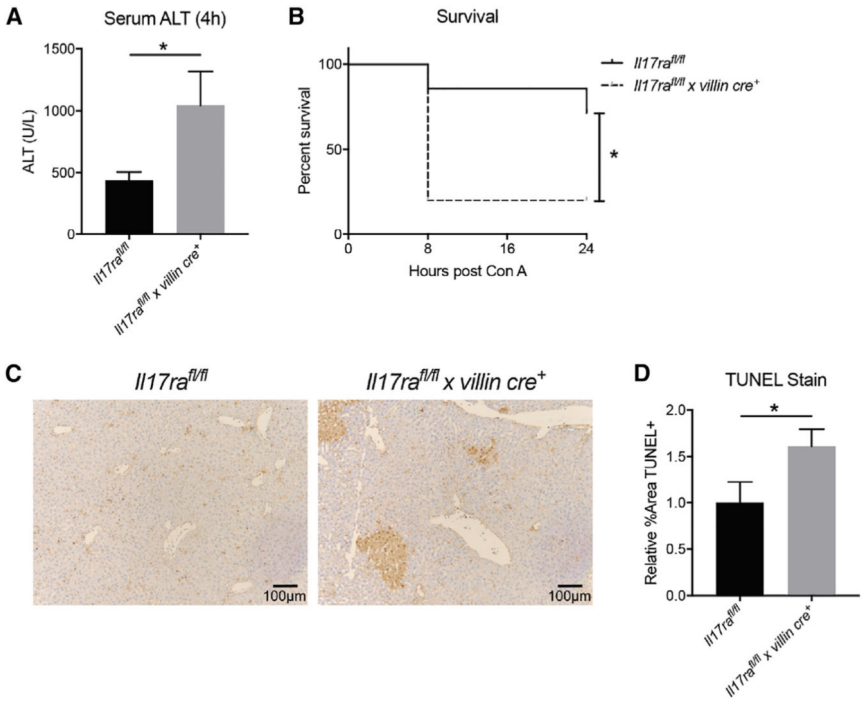

Figure 1. Deletion of IL-17RA in Intestinal Epithelium Exacerbates Concanavalin A Hepatitis

Littermate *Il17ra*$^{fl/fl}$ and *Il17ra*$^{fl/fl}$ × *villin cre*$^{+}$ mice were injected intravenously (i.v.) with concanavalin A (Con A).

(A) Serum alanine aminotransferase (ALT) at 4 h post Con A (10 mg/kg).

(B) Survival curve after 24 h post Con A (10 mg/kg).

(C) Quantification of TUNEL staining at 8 h post Con A (25 mg/kg).

(D) Representative images of TUNEL-stained liver histology at 8 h post Con A (25 mg/kg).

(A, D) Data are represented as mean + SEM.

(n = 5–9 mice/group) (Mann-Whitney test, Gehan-Breslow-Wilcoxon test). p<0.05*, <0.01**, <0.001***, <0.0001****

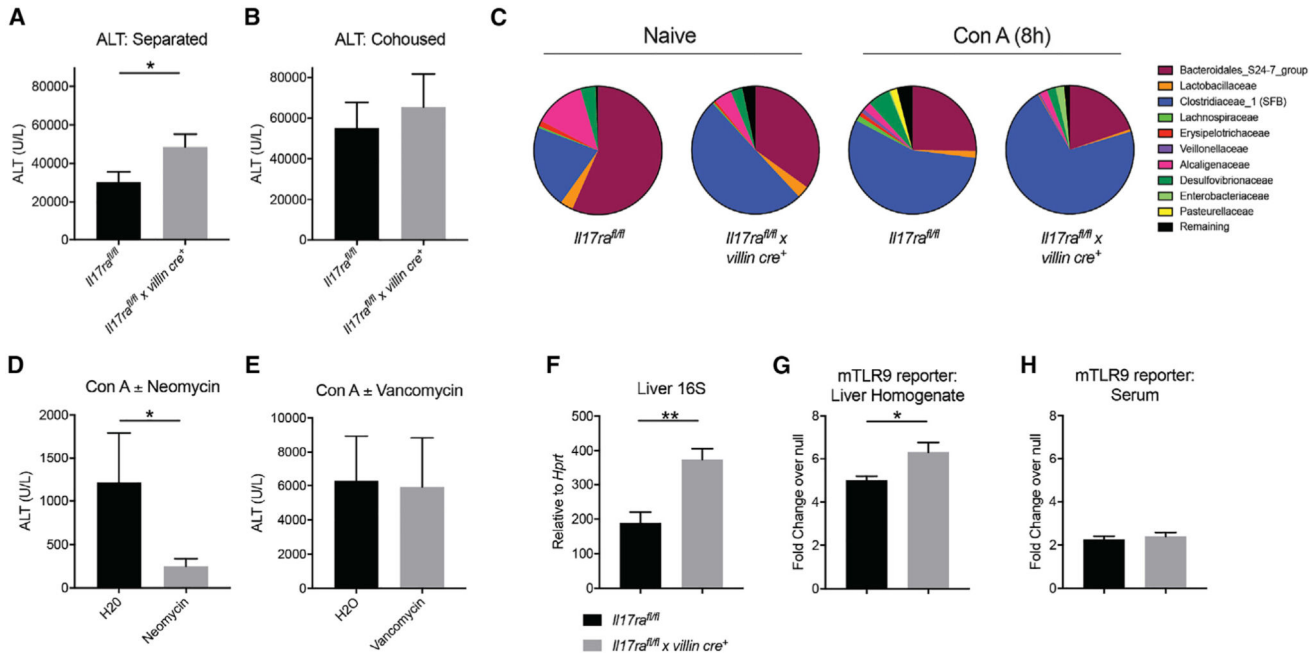

Figure 2. Exacerbated Liver Injury Is Dependent on the Intestinal Microbiota

(A and B) Littermate *Il17ra*$^{fl/fl}$ and *Il17ra*$^{fl/fl}$ × *villin cre*$^{+}$ mice were either cohoused or separated for 1 week. Mice were then treated with concanavalin A (Con A) (25 mg/kg), and serum alanine aminotransferase (ALT) was measured at 8 h (n = 6–14 mice/group).

(C) 16S sequencing on terminal ileum of littermate *Il17ra*$^{fl/fl}$ and *Il17ra*$^{fl/fl}$ × *villin cre*$^{+}$ mice at the naive state and 8 h post Con A (25 mg/kg) (n = 7–16 mice/group).

(D and E) Mice were treated with either 5 days of 1 g/L neomycin (D) or 14 days of 0.5 g/L vancomycin (E) in the drinking water *ad libitum*. Mice were then injected with Con A and serum ALT was measured 8–9 h post injection. (n = 4– mice/group).

(F) 16S rRNA transcript was measured by qRT-PCR in the liver of naive littermate *Il17ra*$^{fl/fl}$ and *Il17ra*$^{fl/fl}$ × *villin cre*$^{+}$ mice (n = 7–10 mice/group).

(G and H) Liver homogenate (G) and serum (H) from naive littermate *Il17ra*$^{fl/fl}$ and *Il17ra*$^{fl/fl}$ × *villin cre*$^{+}$ mice were plated on mTLR9 SEAP reporter cells. Absorbance of supernatants represented as ratio over null/unstimulated cells. (n = 4–8 mice/group).

(A, B, and D–H) Data are represented as mean + SEM.

(unpaired t test; multiple t tests per row; Mann-Whitney test). p<0.05*, <0.01**, <0.001***, <0.0001****

See also Figure S1.

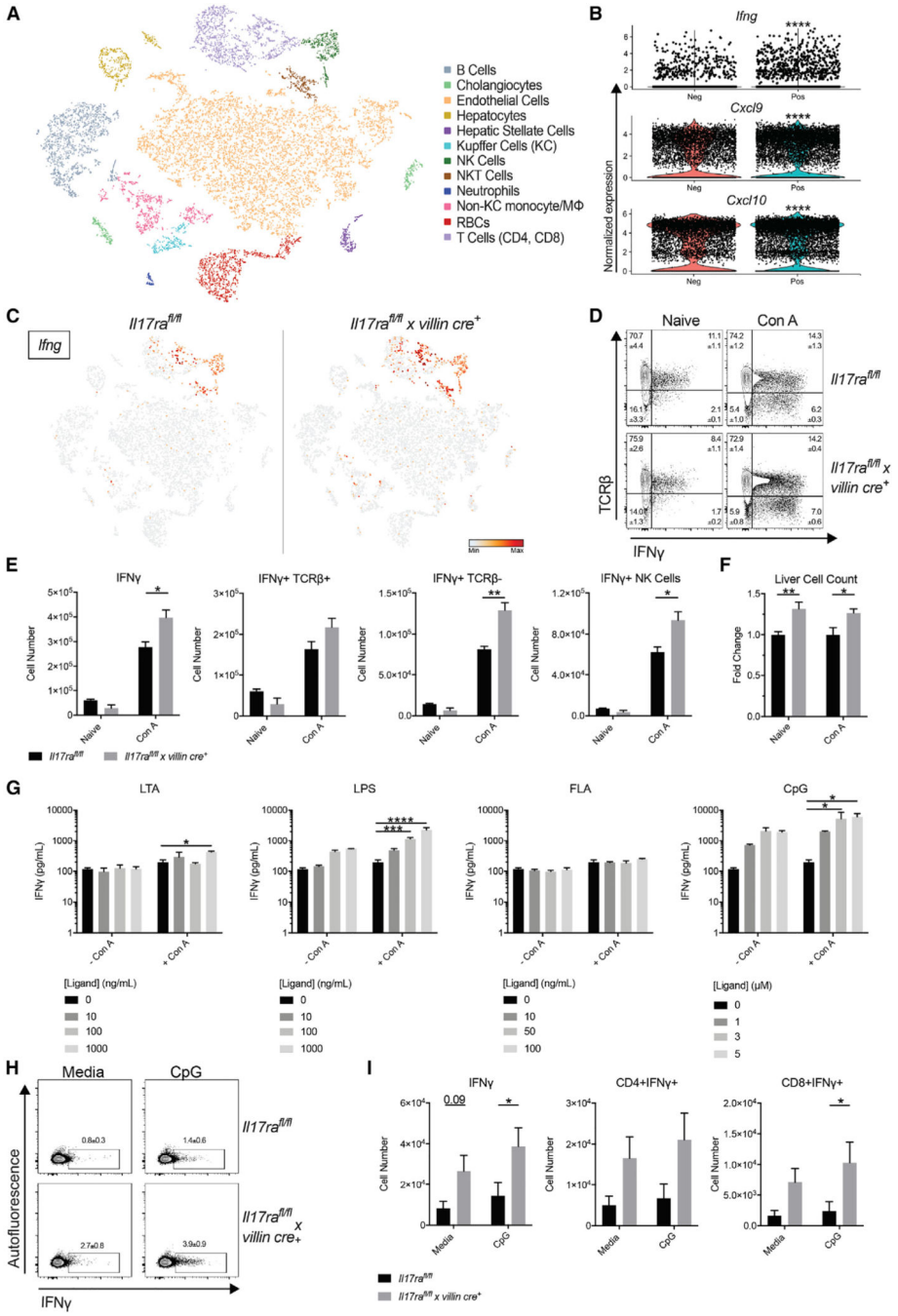

Figure 3. Intestinal IL-17RA Constrains TLR9-Induced Type I Immune Responses in the Liver

(A–C) Ninety minutes after i.v. concanavalin A (25 mg/kg), single-cell RNA sequencing was performed on *Il17ra*$^{fl/fl}$ and *Il17ra*$^{fl/fl}$ × *villin cre*$^{+}$ liver cells enriched for mononuclear cells (n = 2 mice/group). (A) t-Distributed stochastic neighbor embedding (t-SNE) of cell type clustering based on dimensionality reduction and cell-specific gene expression. There is minor overlap between NK and T cell populations. (B) Violin plots of *Ifng, Cxcl9,* and *Cxcl10* log-transformed gene expression in *Il17ra*$^{fl/fl}$ ("Neg") and *Il17ra*$^{fl/fl}$ × *villin cre*$^{+}$

("Pos") liver datasets. See also Figure S5 and Table S1. (C) t-SNE of *Ifng* expressing cells in *Il17ra*$^{fl/fl}$ and *Il17ra*$^{fl/fl}$ × *villin cre*$^{+}$ datasets colored according to relative expression level. (D and E) Flow cytometry analysis of liver cells of littermate *Il17ra*$^{fl/fl}$ and *Il17ra*$^{fl/fl}$ × *villin cre*$^{+}$ mice at the naive state and 5 h post Con A (25 mg/kg) (n = 2–4 mice/group). (D) Representative flow cytometry plots. (E) Number of live IFNγ^{+} cells, IFNγ^{+}TCRβ^{+} cells, IFNγ^{+}TCRβ^{-} cells, and IFNγ^{+} NK Cells (gated on CD90^{+}TCRβ^{-}NK1.1^{+}). (F) Total liver cell number plotted as fold change over *Il17ra*$^{fl/fl}$ (n = 3–16 mice/group). (G) Livers from wild-type *C57BL/6* mice were harvested and enriched for mononuclear cells. Cells were stimulated *ex vivo* with varying concentrations of TLR ligands (lipoteichoic acid [LTA], flagellin [FLA], lipopolysaccharide [LPS], or CpG) ± Con A (5 μg/mL). IFNγ was measured in culture supernatants at 24 h by Luminex (n = 2 replicates/condition). (H and I) Liver mononuclear cells from naive littermate *Il17ra*$^{fl/fl}$ and *Il17ra*$^{fl/fl}$ × *villin cre*$^{+}$ mice were stimulated *ex vivo* with 1 μM CpG for 4 h plus an additional 3 h with brefeldin A and then analyzed by flow cytometry. (H) Representative fluorescence-activated cell sorting (FACS) plots. (I) Number of live IFNγ^{+} cells, CD4^{+} IFNγ^{+} cells (gated on live CD90^{+}TCRβ^{+}), and CD8^{+} IFNγ^{+} cells (gated on live CD90^{+}TCRβ^{+}) (n = 3–4 mice/group). (E–G and I) Data are represented as mean + SEM. (unpaired t test, two-way ANOVA with multiple comparisons, multiple t tests, Wilcoxon rank-sum test). p<0.05*, <0.01**, <0.001***, <0.0001**** See also Figures S2 and S3.

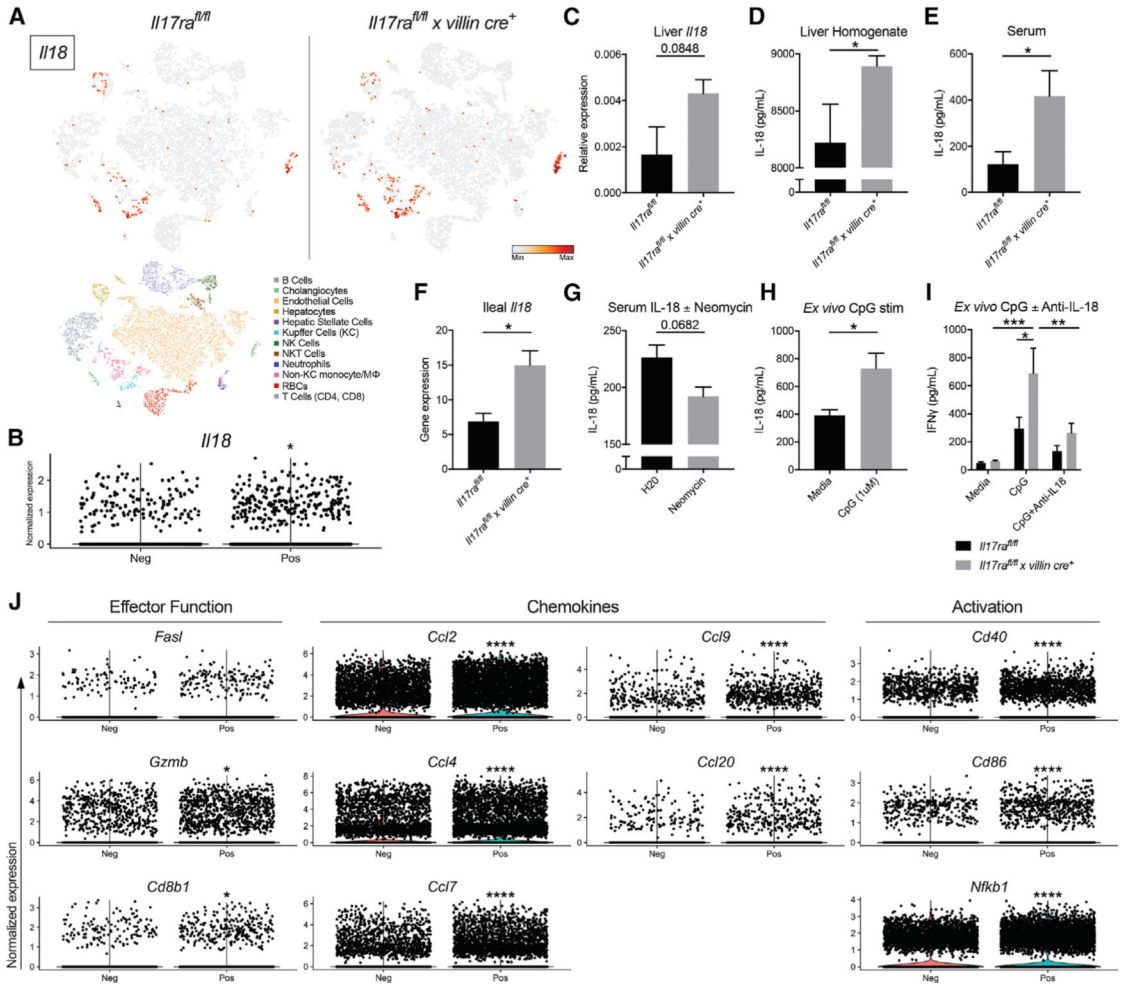

Figure 4. Intestinal IL-17RA Constrains Hepatic and Intestinal IL-18

(A, B, and J) Ninety minutes after IV concanavalin A (25 mg/kg), single-cell RNA sequencing was performed on *Il17ra*$^{fl/fl}$ and *Il17ra*$^{fl/fl}$ × *villin cre*$^{+}$ liver cells enriched for mononuclear cells (n = 2 mice/group). (A) t-SNE of *Il18* expressing cells in *Il17ra*$^{fl/fl}$ and *Il17ra*$^{fl/fl}$ × *villin cre*$^{+}$ liver datasets colored according to relative expression level. t-SNE of cell type clustering for reference (identical to Figure 3A). (B) Violin plot of *Il18* expression (normalized, log-transformed) in *Il17ra*$^{fl/fl}$ ("Neg") and *Il17ra*$^{fl/fl}$ × *villin cre*$^{+}$ ("Pos") liver datasets. (J) Violin plots of various normalized, log-transformed gene expression levels in *Il17ra*$^{fl/fl}$ ("Neg") and *Il17ra*$^{fl/fl}$ × *villin cre*$^{+}$ ("Pos") liver single-cell RNA sequencing 90 min post Con A.

(C–F) In naive littermate *Il17ra*$^{fl/fl}$ and *Il17ra*$^{fl/fl}$ × *villin cre*$^{+}$ mice, liver *Il18* (C), liver IL-18 (D), serum IL-18 (E), and terminal ileum *Il18* (F) was measured.

(G) Serum IL-18 was measured after mice were treated with 5 days of 1 g/L neomycin in drinking water *ad libitum*.

(H and I) Liver cells of naive wild-type *C57BL/6* mice (H) or littermate *Il17ra*$^{fl/fl}$ and *Il17ra*$^{fl/fl}$ × *villin cre*$^{+}$ mice (I) were enriched for mononuclear cells and stimulated with CpG (1 μM) ± anti-IL-18 (5 μg/mL) for 24 h. IL-18 (H) and IFNγ (I) were measured in culture supernatants by ELISA.

(C–I) Data are represented as mean + SEM (n = 3–8 mice/group).
(unpaired t Test, two-way ANOVA with multiple comparisons test, Wilcoxon rank-sum test).
p<0.05*, <0.01**, <0.001***, <0.0001****
See also Figure S5 and Table S1.

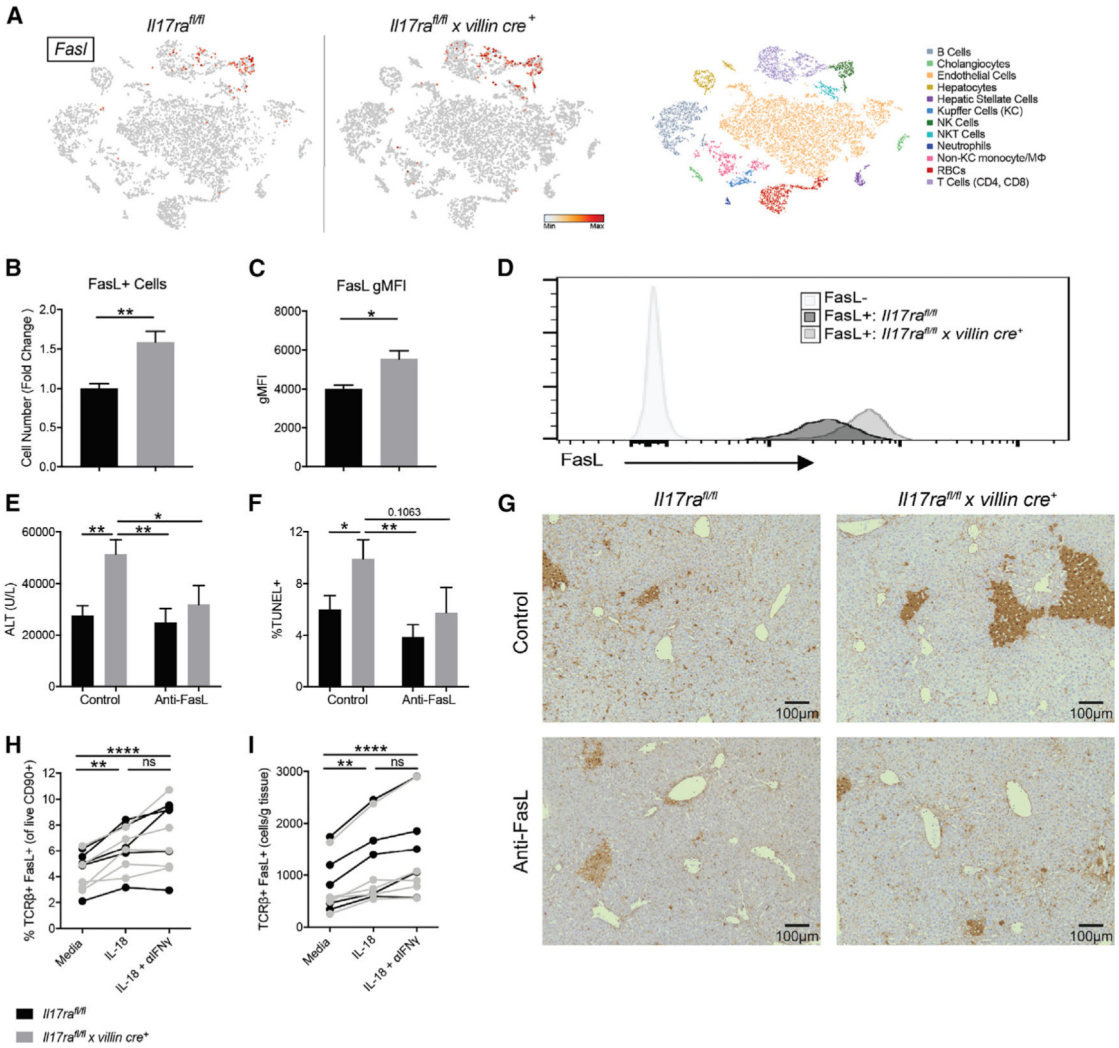

Figure 5. IL-18-Induced Fasl Exacerbates Liver Inflammation

(A) Single-cell RNA sequencing was performed on *Il17ra*$^{fl/fl}$ and *Il17ra*$^{fl/fl}$ × *villin cre*$^{+}$ liver cells enriched for mononuclear cells 90 min post Con A (25 mg/kg) (n = 2 mice/group). t-SNE plots of *Fasl*$^{+}$ cells colored according to relative expression level and reference t-SNE of cell types.

(B–D) Flow cytometry analysis of liver FasL^{+} cells of naive littermate *Il17ra*$^{fl/fl}$ and *Il17ra*$^{fl/fl}$ × *villin cre*$^{+}$ mice (n = 7–11 mice/group). (B) Number of live FasL^{+} cells plotted as fold changeover of *Il17ra*$^{fl/fl}$. (C) FasL geometric mean fluorescence intensity (gMFI) of live FasL^{+} cells. (D) Representative histogram of FasL^{+} cells.

(E–G) Wild-type controls and *Il17ra*$^{fl/fl}$ × *villin cre*$^{+}$ mice (n = 6–28 mice/group) were treated with i.v. anti-FasL (250–500 μg/mouse) 1 h prior to i.v. Concanavalin A (25 mg/kg). Serum alanine aminotransferase (ALT) (E) and TUNEL staining (F) was analyzed 8 h post Con A. (G) Representative images of TUNEL-stained liver.

(H and I) Liver mononuclear cells from naive littermate *Il17ra*$^{fl/fl}$ and *Il17ra*$^{fl/fl}$ × *villin cre*$^{+}$ mice were stimulated *ex vivo* with 50 ng/mL IL-18 ± 5 μg/mL anti-IFNγ (αIFNγ) and

analyzed by flow cytometry. Percent (H) and actual number (I) of TCRβ^{+}FasL^{+} cells (gated on live CD90^{+} cells). Lines connect paired samples. Each dot/line represents one mouse. (B, C, E, and F) Data are represented as mean + SEM.
(unpaired t test, one-way ANOVA with multiple comparisons test, two-way ANOVA with multiple comparisons test). p<0.05*, <0.01**, <0.001***, <0.0001****

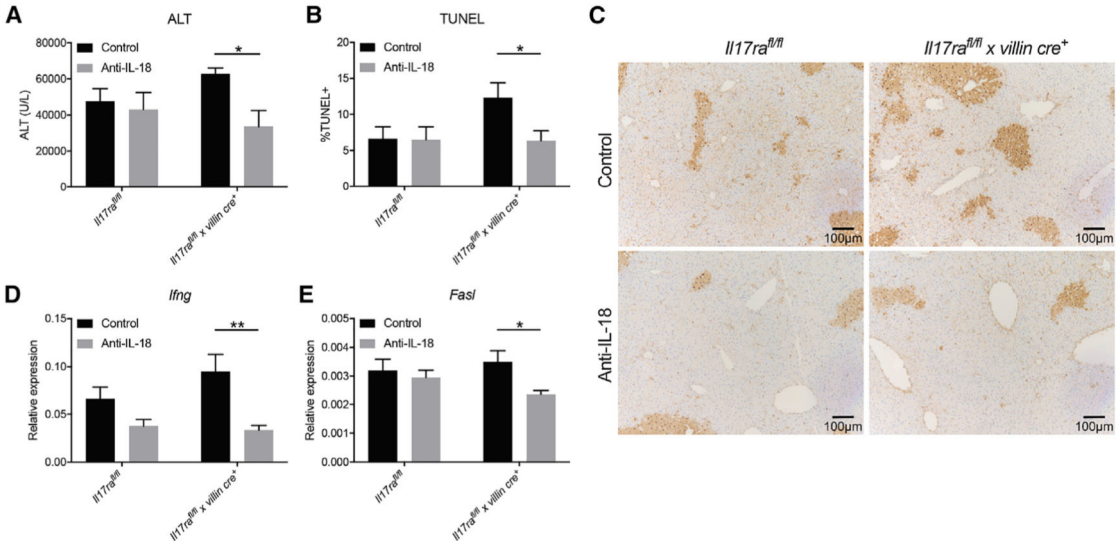

Figure 6. Anti-IL18 Mitigates Liver Injury in Intestinal Il17RA-Deficient Mice

Littermate *Il17ra*$^{fl/fl}$ and *Il17ra*$^{fl/fl}$ × *villin cre*$^{+}$ mice were pre-treated with anti-IL-18 (0.5 mg/mouse) 1 day prior to IV concanavalin A (Con A) (25 mg/kg) and sacrificed at 8 h post Con A (n = 7–9 mice/group).

(A) Serum alanine aminotransferase (ALT).

(B) Quantification of TUNEL staining.

(C) Representative images of TUNEL-stained liver histology.

(D and E) Liver *Ifng* (D) and *Fasl* (E) gene expression as measured by qRT-PCR. (A–B, D–E) Data are represented as mean + SEM (one-way ANOVA with multiple comparisons test). p<0.05*, <0.01**, <0.001***, <0.0001****

KEY RESOURCES TABLE

REAGENT or RESOURCE	SOURCE	IDENTIFIER
Antibodies		
Anti-IL-18	Genentech	N/A
Anti-mouse IFNγ	BioXCell	Cat#BE0055-A025mg; RRID: AB_1107694
Anti- mouse FasL	BioLegend	Cat#93971; RRID: AB_313281
IgG Isotype Control	BioLegend	Cat#92257, RRID: AB_11203529
BV786 Anti-mouse CD4	BD Biosciences	Cat#563727; RRID: AB_2728707
APC Anti-mouse IFNγ	eBioscience	Cat#17–7311–82; RRID: AB_469504
APCe780 Anti-mouse TCRβ	eBioscience	Cat#47–5961–82; RRID: AB_1272173
BV421 Anti-mouse NK1.1	BD Biosciences	Cat#562921; RRID: AB_2728688
BV395 Anti-mouse CD3	BD Biosciences	Cat#563565; RRID: AB_2738278
PCP-Cy5 Rat-Anti-Mouse CD3 Molecular Complex	BD Biosciences	Cat#560527; RRID: AB_1727463
BV605 Anti-Mouse CD90.2	BD Biosciences	Cat#740334; RRID: AB_2740067
PE Anti-Mouse FasL	BioLegend	Cat#106606; RRID: AB_313279
PE-Cy7 Anti-mouse CD8	eBiosciences	Cat#25–0083–82; RRID: AB_11218494
Anti-Mouse CD16/CD32	eBiosciences	Cat#14–0161–86; RRID: AB_467135
PE anti-mouse IgA	eBiosciences	Cat#12–4204–81; RRID: AB_465916
Chemicals, Peptides, and Recombinant Proteins		
Concanavalin A from *Canavalia ensiformis* (jack bean) type IV	Sigma-Aldrich	Cat#C2010
Ultrapure LPS, *E. coli* 0111:B4	Invivogen	Cat#lrl-3pelps
Purified LTA from S. aureus	Invivogen	Cat#tlrl-pslta
TLR9 Agonist - Stimulatory CpG ODN, Class C, Human / mouse	Invivogen	Cat#tlrl-2395
Ultrapure flagellin from B. subtilis	Invivogen	Cat#tlrl-pbsfla
E. coli dsDNA	Invivogen	Cat#tlrl-ecdna
Critical Commercial Assays		
ALT Activity Assay	Sigma-Aldrich	Cat#MAK052
ApopTag® Peroxidase *In Situ* Apoptosis Detection Kit	Millipore Sigma	Cat#S7100
Mouse IFN-γ ELISA	BioLegend	Cat#430804
Mouse IL-18 ELISA	Invitrogen	Cat# BMS618–3; RRID: AB_2575692
Pierce BCA Protein Assay Kit	Thermo Scientific	Cat# 23225
Chromium™ Single Cell 3′ Gel Bead Kit v2	10x Genomics	Cat# PN-120235
MinElute PCR Purification Kit	QIAGEN	Cat#28004
Purelink PCR Purification Kit	Life Technologies	Cat#K310001
MiSeq Reagent Kit v2 (500-cycles)	Illumina	Cat#MS-102–2003
LIVE/DEAD Fixable Aqua Dead Cell Stain Kit	Invitrogen	Cat#L34966
MILLIPLEX Mouse Th17 Magnetic Bead Panel	Millipore Sigma	Cat#MTH17MAG-47K
Cytokine & Chemokine 36-Plex Mouse Procarta Plex Panel 1A	Thermo Fisher Scientific-Affymetrix	Cat#EPX360–26092–901; RRID: AB_2576123

REAGENT or RESOURCE	SOURCE	IDENTIFIER
Deposited Data		
Liver Single Cell RNA sequencing	This Paper	GEO: GSE128284
16S rRNA sequencing	This Paper	SRA BioProject: PRJNA526489
Terminal ileum RNA sequencing	Kumar et al., 2016	SRA: SRP069071
Experimental Models: Cell Lines		
HEK-Blue mTLR9 cells	Invivogen	Cat#hkb-mtlr9
HEK-Dual mTLR4 cells	Invivogen	Cat#hkd-mtlr4ni
Experimental Models: Organisms/Strains		
Mouse: *C57BL/6*	Taconic Biosciences	C57BL/6NTac
Mouse: *Il17ra*$^{fl/fl}$	Kumar et al., 2016	MGI:5907986
Mouse: *Il17ra*$^{fl/fl}$ *x villin cre*$^{+}$	Kumar et al., 2016	N/A
Mouse: *Nlrc4*^{mut}	Weiss et al., 2018	N/A
Mouse: *Nlrc4*^{mut}*Il18bp*$^{-/-}$	Courtesy of collaborator, Dr. Scott Canna	N/A
Mouse: *Il18bp*$^{-/-}$	UC Davis KOMP Repository	MGI:1333800
Oligonucleotides		
Primer for 16S rDNA: Forward (Eubact Uni340FP) - ACTCCTACGGGAGGCAGCAGT, Reverse (Eubact Uni514RP)- ATTACCGCGGCTGCTGGC	Croswell et al., 2009; Salzman et al., 2010; Kumar et al., 2016	N/A
Primer: mouse *Hprt*	Integrated DNA Technologies	Cat# Mm.PT.39a.22214828
Primer: mouse *Ifng*	Applied Biosystems (Thermo Fisher Scientific)	Cat#Mm01168134_m1
Primer: mouse *Il18*	Applied Biosystems (ThermoFisher Scientific)	Cat#Mm00434226_m1
Primer: mouse *FasL*	Applied Biosystems (ThermoFisher Scientific)	Cat#Mm00438864_m1
Software and Algorithms		
Cell Ranger version 2.1.1	10x Genomics	https://support.10xgenomics.com/single-cell-gene-expression/software/pipelines/latest/what-is-cell-ranger
Seurat suite version 2.2.1	Satija Lab	https://satijalab.org/seurat/
Loupe Browser	10x Genomics	https://support.10xgenomics.com/single-cell-gene-expression/software/visualization/latest/what-is-loupe-cell-browser
Prism	Graphpad	https://www.graphpad.com/scientific-software/prism/
Mothur	Schloss et al., 2009	N/A
R package	Tarabichi et al., 2015	N/A
FlowJo version 10	Flowjo	https://www.flowjo.com
ImageJ	NIH	https://imagej.nih.gov/ij/index.html
Other		
Trizol	Life Technologies	Cat#15596–018
Trizol LS	Life Technologies	Cat#10296010
iScript Reverse Transcription Supermix	Bio-RAD	Cat#1708841

REAGENT or RESOURCE	SOURCE	IDENTIFIER
SSoFast Supermix	Bio-RAD	Cat#1725281
SYBR Green Supermix	Bio-RAD	Cat#1708880
Roche cOmplete Protease Inhibitor Cocktail	Signma Aldrich	SKU: 11697498001
QUANTI-Blue:Alkaline phosphatase detection medium - Powder	Invivogen	Cat#rep-qb1
IMDM, GlutaMAX Supplement	Thermo Fisher Scientific	Cat#31980097
FBS	Thermo Fisher Scientific	Cat#A3160502
Penicillin-Streptomycin-Glutamine (100X)	Thermo Fisher Scientific	Cat#10378016
Collagenase	Sigma Aldrich	Cat#C5138–500MG
DNase I	Sigma Aldrich	Cat#11284932001
Percoll	Fisher Scientific	Cat#45001747
Q5 HS High-Fidelity polymerase	New England BioLabs	Cat# M0493L
AMPure XP for PCR Purification	Beckman Coulter Life Sciences	Cat#A63881
Hoechst 33342	Life Technologies	Cat#H3570
Normal Rat serum	Thermo Fisher Scientific	Cat#01–9601; RRID: AB_2532968
AccuCheck Cell Counting Beads	Thermo Fisher Scientific	Cat#pcb100
Brefeldin A	eBioscience	Cat#00–4506–51
FITC Dextran 4k	Sigma Aldrich	Cat#FD4–1G